ACS APPLIED MATERIALS & INTERFACES

www.acsami.org

Research Article

Hyaluronic Acid Hydrogels with Phototunable Supramolecular Cross-Linking for Spatially Controlled Lymphatic Tube Formation

Fei Fan, Bo Su, Alexander Kolodychak, Ephraim Ekwueme, Laura Alderfer, Sanjoy Saha, Matthew J. Webber,* and Donny Hanjaya-Putra*

Cite This: *ACS Appl. Mater. Interfaces* 2023, 15, 58181−58195

Read Online

ACCESS | Metrics & More | Article Recommendations | Supporting Information

ABSTRACT: The dynamics of the extracellular matrix (ECM) influences stem cell differentiation and morphogenesis into complex lymphatic networks. While dynamic hydrogels with stress relaxation properties have been developed, many require detailed chemical processing to tune viscoelasticity, offering a limited opportunity for *in situ* and spatiotemporal control. Here, a hyaluronic acid (HA) hydrogel is reported with viscoelasticity that is controlled and spatially tunable using UV light to direct the extent of supramolecular and covalent cross-linking interactions. This is achieved using UV-mediated photodimerization of a supramolecular ternary complex of pendant *trans*-Brooker's Merocyanine (BM) guests and a cucurbit[8]uril (CB[8]) macrocycle. The UV-mediated conversion of this supramolecular complex to its covalent photodimerized form is catalyzed by CB[8], offering a user-directed route to spatially control hydrogel dynamics in combination with orthogonal photopatterning by UV irradiation through photomasks. This material thus achieves spatial heterogeneity of substrate dynamics, recreating features of native ECM without the need for additional chemical reagents. Moreover, these dynamic hydrogels afford spatial control of substrate mechanics to direct human lymphatic endothelial cells (LECs) to form lymphatic cord-like structures (CLS). Specifically, cells cultured on viscoelastic supramolecular hydrogels have enhanced formation of CLS, arising from increased expression of key lymphatic markers, such as *LYVE-1*, *Podoplanin*, and *Prox1*, compared to static elastic hydrogels prepared from fully covalent cross-linking. Viscoelastic hydrogels promote lymphatic CLS formation through the expression of *Nrp2*, *VEGFR2*, and *VEGFR3* to enhance the VEGF-C stimulation. Overall, viscoelastic supramolecular hydrogels offer a facile route to spatially control lymphatic CLS formation, providing a tool for future studies of basic lymphatic biology and tissue engineering applications.

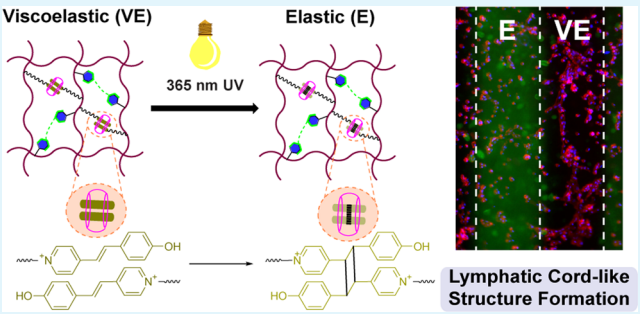

KEYWORDS: *hyaluronic acid, supramolecular hydrogels, host−guest chemistry, viscoelasticity, lymphatic morphogenesis*

1. INTRODUCTION

Tissues and organs are complex and hierarchically organized systems with numerous biochemical and biophysical cues that are responsive to exogenous or endogenous signals arising from healthy and pathological processes. Stem cell differentiation and tissue morphogenesis arise from dynamic biophysical cues, offering inspiration for the design of materials for tissue engineering applications.[1−3] In native tissues, the biophysical features of the extracellular matrix (ECM) play important roles in maintaining homeostasis. The ECM of a wide variety of biological tissues like skin, muscle, heart, and brain exhibit nonlinear elastic behavior.[4,5] The viscoelastic properties of these tissues enable adaptation to mechanical deformation and underlying processes, such as matrix remodeling. In disease development, the change in matrix viscoelasticity offers a supplementary indicator for use in diagnosis and evaluation.[6,7] Harnessing viscoelasticity in the construction of biomaterials thus presents a route to mimic the mechanical dynamics of native ECM to enable the biophysical control of processes such as cell spreading, proliferation, migration, and differentiation.

Dynamic viscoelastic hydrogels have been developed to recreate the mechanical dynamics of native ECM. Hydrogel viscoelasticity is achieved by dynamic modes of cross-linking, including dynamic-covalent bonds and noncovalent interactions.[8,9] Host−guest supramolecular interactions enable a route to dynamically cross-link hydrogels, realizing materials with a dynamic bond exchange that is then manifest in tunable stress relaxation times on the bulk scale;[10−12] these properties can be further tuned by combining host−guest interactions with covalent cross-linking.[12−14] Ionic gelation of alginate

Received: August 24, 2023
Revised: November 23, 2023
Accepted: November 27, 2023
Published: December 8, 2023

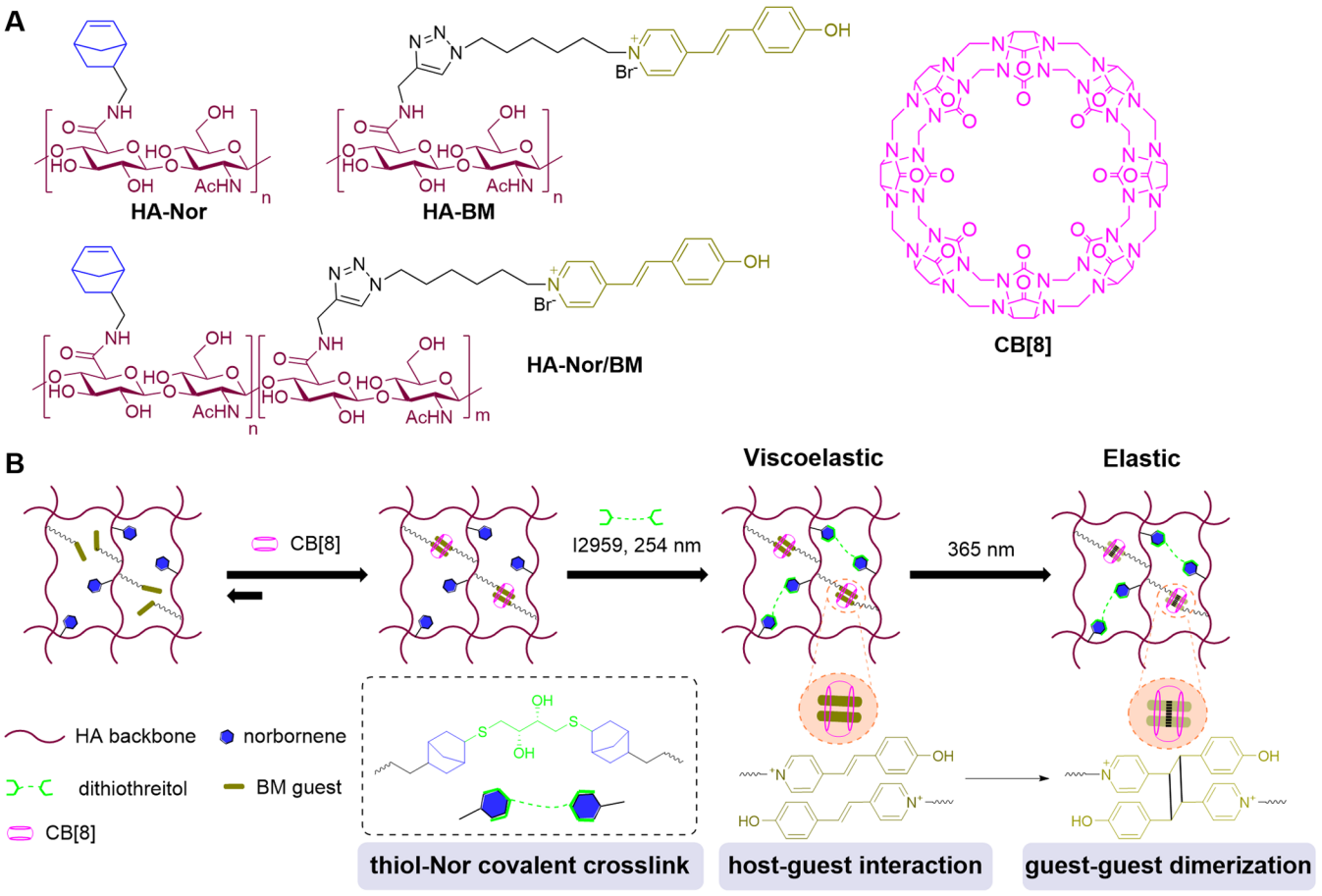

Figure 1. Light-controlled viscoelastic hydrogels based on supramolecular BM_2⊂CB[8] interaction and thiol-Nor covalent cross-linking. (A) Chemical structures of norbornene-modified hyaluronic acid (HA-Nor), *trans*-Brooker's merocyanine (BM)-modified HA (HA-BM), Nor and BM-modified HA (HA-Nor/BM), and the cucurbit[8]uril macrocycle (CB[8]). (B) Adding CB[8] to HA-Nor/BM polymer solutions promotes supramolecular cross-linking via the formation of a host−guest BM_2⊂CB[8] ternary complex. Upon irradiation with 254 nm UV light in the presence of dithiothreitol (DTT) and photoinitiator Irgacure 2959 (I2959), thiol-Nor covalent cross-linking is introduced to form a viscoelastic hydrogel comprised of both supramolecular and covalent cross-links. Further irradiation with 365 nm UV light induces photodimerization of BM guests within the CB[8] portal to convert the remaining supramolecular cross-links to covalent cross-links. Therefore, the conversion of a viscoelastic hydrogel to an elastic hydrogel can be precisely controlled by UV light.

using calcium offers another route to prepare hydrogels with slow stress relaxation, with the density of covalently grafted poly(ethylene glycol) (PEG) chains on alginate offering a route to precisely tune viscoelasticity.[15] Boronate esters formed from phenylboronic acids and diols are one type of dynamic-covalent interaction;[16−18] mixing multiple boronate esters with distinct kinetics affords hierarchical mechanical tuning of hydrogels.[19]

Although an increase in stiffness can lead to increases in cell spreading and proliferation, stress relaxation also promotes the spreading and proliferation of cells[20,21] as well as the differentiation of human multipotent mesenchymal stromal cells (hMSCs) toward smooth muscle cells.[22] Faster stress relaxation promotes volume expansion of MSCs[23] and thus leads to enhanced osteogenesis[24] in hydrogels with an initial elastic modulus of ∼20 kPa. Additionally, in alginate hydrogels with identical initial elastic modulus, fast stress relaxation and high adhesion density promote viability, proliferation, and lumen formation of human induced pluripotent stem cells (hiPSCs).[25] Furthermore, viscoelasticity shows interesting effects on vascular morphogenesis. It was reported that dynamic hydrogels enabled rapid vascular morphogenesis in a stiffness-independent manner through the activation of focal adhesion kinase (FAK) and matrix remodeling by metalloproteinases.[26] These studies therefore point to the impact of tuning the viscoelasticity of synthetic ECM mimics through the type and density of cross-linking, with the possibility to direct the phenotype and fate of cultured cells. At the same time, most of the reported viscoelastic hydrogels explored for this purpose are static, and as such, the tuning of viscoelasticity can only be achieved through *a priori* chemical design and/or fine adjustment of the cross-linking ratio. Accordingly, protocols to realize bulk hydrogels with *in situ* and spatiotemporal control of viscoelasticity remain limited.

Here, we designed hydrogels with spatially controlled and tunable viscoelasticity, leveraging a combination of supramolecular and covalent cross-linking on a hyaluronic acid (HA) backbone (Figure 1). To afford supramolecular cross-linking, HA was modified with pendant *trans*-Brooker's Merocyanine (BM) groups that form homoternary complexes with free cucurbit[8]uril (CB[8]) macrocycles; this supramolecular homoternary complex can be further converted to a covalent cross-linking interaction by the formation of a [2 + 2] photodimer upon exposure with UV light.[27,28] Since HA cross-linked with only BM_2⊂CB[8] supramolecular ternary complexes had rapid stress relaxation and dissipated in water, we

https://doi.org/10.1021/acsami.3c12514
ACS Appl. Mater. Interfaces 2023, 15, 58181−58195

Table 1. Synthesis of HA-BM and HA-Nor/BM by Copper-Catalyzed Cycloadditions of BM-Azide to Alkyne-Functionalized Hyaluronic Acid[a]

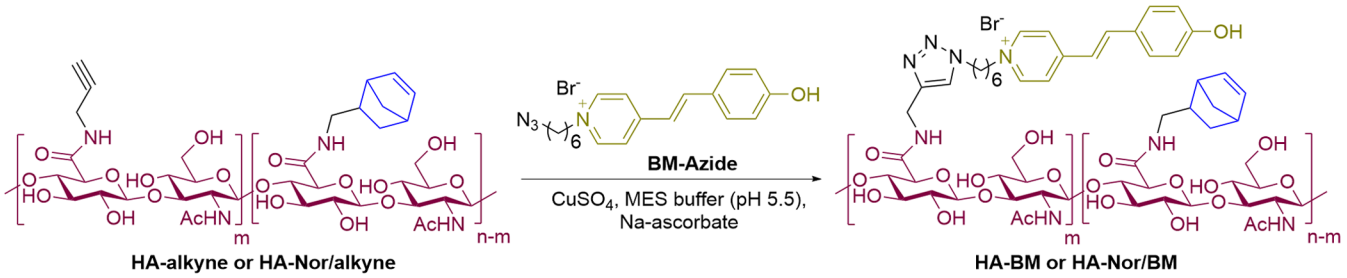

entry	DS of alkyne (%)[b]	DS of Nor (%)[c]	alkyne conv. (%)	DS of BM (%)[f]	product
1	18	0	100[d]	18	**HA-BM**
2	18	8	100	18	**HA-Nor/BM**
3	18	20	ND[e]		
4	22	18	ND		
5	30	0	ND		
6	30	15	ND		
7	10	30	100	10	
8	12	38	ND		

[a]Reactions were performed at room temperature under nitrogen. [b]The degree of substitution (DS) of alkyne, based on the carboxyl group of the HA backbone. [c]The degree of substitution (DS) of norbornene, based on the carboxyl group of the HA backbone. [d]Alkyne conversion was determined by the disappearance of the alkyne signal (2.66 ppm) on ^{1}H NMR. [e]Not detected due to precipitation or product dispersed in deionized (DI) H_2O as hydrogel aggregates. [f]The degree of substitution (DS) of BM is equal to the degree of substitution of alkyne as alkyne conversion is 100%.

also modified HA with norbornene (Nor) to enable covalent cross-linking by difunctional thiol molecules through the thiol-Nor reaction induced by 254 nm UV light. This thiol-Nor chemistry has been previously applied for orthogonal and gradient photopatterning of hydrogels,[29,30] and the strained Nor groups have high reaction efficiency and selectivity for thiol groups under free radical conditions. The combination of covalent thiol-Nor bonding and supramolecular BM_2⊂CB[8] ternary cross-links thus afforded the formation of a viscoelastic hydrogel. The BM_2⊂CB[8] complex could then be irradiated with 365 nm UV light to convert this motif into a covalent cross-link, resulting in the transition from a viscoelastic hydrogel to a completely covalent cross-linked elastic hydrogel. Furthermore, spatiotemporal control of viscoelasticity and orthogonal photopatterning were achieved by UV irradiation using photomasks without the need for additional chemical reagents to alter cross-linking. This provided a facile and minimally disruptive way to tune viscoelasticity at the microscale without the addition of chemical reagents that may impact biological outcomes. We demonstrated that these dynamic hydrogels could provide spatial control over human lymphatic endothelial cells (LECs) to form lymphatic cord-like structures (CLS), with the viscoelastic hydrogels supporting CLS formation by promoting the expression of key lymphatic markers.

2. RESULTS AND DISCUSSION

2.1. Synthesis of HA-Nor, HA-BM, and HA-Nor/BM. In this study, an HA backbone was modified with pendant Nor and BM groups to introduce covalent and supramolecular cross-linking interactions, respectively. HA is a critical component of the ECM and has been demonstrated to be biocompatible and nonimmunogenic when used as a biomaterial; it is also amenable to facile chemical modification via its carboxyl groups as well as primary and secondary hydroxyl groups.[31,32] Specifically, the carboxyl and primary hydroxyl groups are more reactive than the secondary hydroxyl groups, enabling routes for modification by ester, amide, and ether linkages. Compared with ester bonds, amide bonds are more stable with limited hydrolysis. Therefore, the Nor and BM groups were grafted onto HA using amide linkages. The Nor and BM groups enable orthogonal cross-linking interactions by the addition of dithiol through thiol-Nor bonds and CB[8] for BM_2⊂CB[8] ternary complex formation. Nor and BM modification of HA could be performed on either the same (HA-Nor/BM) or separate (HA-Nor and HA-BM) polymer chains. Modifying Nor and BM groups on separate HA polymer chains (HA-Nor and HA-BM) introduces the ability to form a double-network hydrogel while modifying Nor and BM groups on the same HA polymer chain (HA-Nor/BM) can afford a dual-cross-linked hydrogel (Figure S1). Both dual-cross-linked and double-network hydrogels were investigated in this work, offering options for materials design in future applications.

HA modification was achieved using 4-(4,6-dimethoxy-1,3,5-triazin-2-yl)-4-methylmorpholinium chloride (DMTMM)[33,34] as this agent is aqueous soluble and has higher reaction efficiency than most conventional coupling reagents. HA-Nor was synthesized via a one-step reaction with 5-norbornene-2-methylamine, and the ^{1}H NMR spectrum showed the degree of substitution (DS) to be 23% (Scheme S2A). HA-BM was synthesized by first modifying HA with propargylamine and then appending an azide-modified BM group (Scheme S1) through copper-catalyzed azide−alkyne cycloaddition (CuAAC) (Scheme S2B). The complete reaction of HA-alkyne with BM azide was confirmed by the disappearance of the alkyne signal in the ^{1}H NMR spectrum (2.66 ppm) and no fluorescence or absorbance from exposure to a thiol-containing rhodamine derivative under conditions favoring a thiol-alkyne Michael-type addition (Figure S4B,C). HA-BM with DS of 18% was readily synthesized (Table 1, entry 1); when the DS

https://doi.org/10.1021/acsami.3c12514
ACS Appl. Mater. Interfaces 2023, 15, 58181−58195

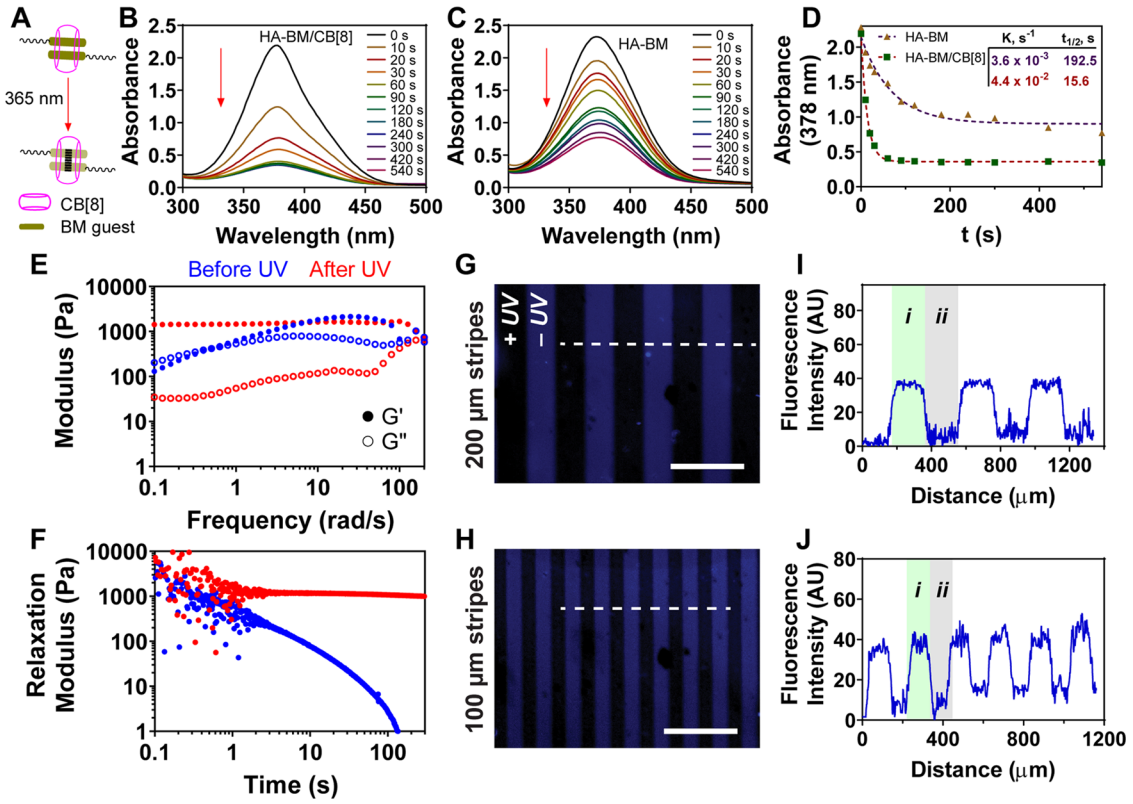

Figure 2. Photodimerization of HA-BM by addition of CB[8]. (A) Schematic of photodimerization of the supramolecular BM_2⊂CB[8] complex using 365 nm UV light. Absorbance spectra of HA-BM dimerization over time (B) with or (C) without the addition of CB[8], (D) maximum absorbance was fit to a first-order rate equation with fit parameters shown in the inset. (E) Frequency sweep rheology at 2% strain for hydrogel of HA-BM with CB[8] at 20 mg mL^{-1} before (blue) and after (red) UV irradiation. (F) Stress relaxation modulus with 10% strain for hydrogel of HA-BM with CB[8] at 20 mg mL^{-1} before (blue) and after (red) UV irradiation. Photopatterning of HA-BM/CB[8] hydrogel with a photomask of (G) 200 μm and (H) 100 μm stripes. The patterns were imaged by 4′,6-diamidino-2-phenylindole (DAPI) (blue) filters of a microscope to show the conversion of (i) the BM_2⊂CB[8] host−guest interaction to (ii) the covalent photodimerized BM using 365 nm UV light. Scale bars: 500 μm. Fluorescence intensity profiles of blue colors were quantified along the dashed white line for (I) 200 μm and (J) 100 μm stripe patterns.

was increased to 30%, precipitates were formed during CuAAC (Table 1, entry 5). For HA-Nor/BM synthesis, HA was modified with Nor and alkyne groups through one-pot amidation with BM guests subsequently grafted using CuAAC (Scheme S2C). HA-Nor/BM was synthesized with a low DS value of 8% for Nor and 18% for BM (Table 1, entry 2), but increasing the DS value of Nor (Table 1, entries 3 and 4) resulted in precipitation during CuAAC. Lyophilized products were dispersed in water in the form of small hydrogels (Figure S2). In addition, HA-Nor/BM with 30% Nor and 10% BM DS was obtained (Table 1, entry 7), but the higher DS value resulted in precipitation (Table 1, entry 8). We expect that precipitates form at high DS values due to the hydrophobic interaction of Nor and BM, along with the concomitant loss of key solubilizing carboxylate groups on HA upon modification with these pendants.

In summary, we synthesized HA-Nor with a 23% DS value, HA-BM with an 18% DS value, HA-Nor/BM with a low DS value of 8% for Nor and 18% for BM, and HA-Nor/BM with a high DS value of 30% for Nor and 10% for BM. Modulation of the DS value of Nor and BM alters the ratio of covalent and supramolecular cross-linking and thus leads to control over hydrogel dynamics and stiffness. Either the low or high DS HA-Nor/BM can be used according to the needs of further applications. However, to prepare hydrogel with fast dynamics, HA-Nor/BM with a low DS of 8% for Nor and 18% for BM was used for phototunable viscoelastic hydrogel preparation and cell culture.

2.2. Supramolecular Interaction between HA-BM and CB[8]. The supramolecular cross-linking of HA by BM_2⊂CB[8] ternary complexes was first investigated in deionized water (DI H_2O) at various molar ratios of CB[8] to BM. The theoretical CB[8]:BM stoichiometric ratio for the ternary complex is 0.5. Absorbance spectra of 0.5 mg mL^{-1} HA-BM (192 μM BM) exhibited a red-shift with an increasing molar ratio of CB[8]:BM (Figure S3A), with λ_{max} shifting from 374 nm (without CB[8]) to 396 nm (excess CB[8]). The red-shifting of λ_{max} may be attributed to the breakdown of BM stacking in the CB[8] cavity by excess CB[8] to form the 1:1 CB[8]:BM complex. The absorbance decreased as the CB[8]:BM ratio was increased from 0 to 0.48, and subsequently increased as the CB[8]:BM ratio continued to increase to 1.21. The decrease in absorbance suggests the complete formation of the homoternary complex around the expected ratio of CB[8]:BM of 0.5, where the BM motifs are maximally coupled within the CB[8] cavity. The subsequent increase in absorbance once CB[8] is in excess (CB[8]:BM > 0.5) arises from an increased prevalence of 1:1 CB[8]:BM complex formation. While this has been previously reported to be a cooperative ternary complex ($K_{eq,1}$ = 2.95 × 10^5 M^{-1}, $K_{eq,2}$ = 2.88 × 10^6 M^{-1}) in the soluble form,[35] the polymer-bound guest may introduce considerations related to polymer entropy that reduce complex cooperativity and favor more 1:1 complex

https://doi.org/10.1021/acsami.3c12514
ACS Appl. Mater. Interfaces 2023, 15, 58181−58195

formation between CB[8] and BM, especially in cases of excess CB[8]. The ratio of absorbance at 396 to 374 nm was constant when the CB[8] molar ratio was lower than 0.40 and then gradually increased until reaching a plateau at CB[8]:BM ratios beyond 0.8 (Figure S3B), further supporting some conversion of the homoternary complex to a binary complex under conditions of excess CB[8].

2.3. HA-BM and CB[8] Supramolecular Hydrogel. After verifying the optimal CB[8]:BM molar ratio needed to form the homoternary complex, CB[8]-catalyzed photodimerization of encapsulated BM guests was next investigated under dilute subgelation conditions using 365 nm UV irradiation (Figure 2A). At a CB[8]:BM molar ratio of 0.5 and a polymer concentration of 0.5 mg mL^{-1} HA-BM (192 μM BM), absorbance spectra collected over time supported a progression in photodimerization upon increased exposure to UV irradiation (Figure 2B). HA-BM photodimerization still occurred in the absence of CB[8] (Figure 2C). A comparison of the kinetics of this process (Figure 2D) indicated a catalytic role for CB[8] ($t_{1/2}$ of 15.6 s and rate constant K of 4.4×10^{-2} s^{-1}) compared to the case when CB[8] was absent ($t_{1/2}$ of 192.5 s and K of 3.6×10^{-3} s^{-1}). The dimerization seen for HA-BM in the absence of CB[8] was unexpected, as a similar result was not obtained when BM was appended from 4-arm PEG macromers,[27] though a pluronic-based system that was more prone to aggregation did show some extent of BM dimerization in the absence of CB[8].[28] Compared to the presentation of BM on flexible PEG macromers, the modification of BM onto a structured polymer like HA would be expected to shorten its distance and facilitate increased self-aggregation via $\pi-\pi$ stacking and hydrophobic interactions of the BM groups, likely leading to some UV-induced dimerization even without the addition of CB[8]. A different guest appended onto HA that also participated in a CB[8]-catalyzed photodimerization reaction was previously shown to aggregate and promote gelation even without the addition of the CB[8] macrocycle.[36] Guest aggregation also likely underlies the precipitation previously mentioned for HA modified with a BM at a DS of 30%.

Next, the change in fluorescence of HA-BM over time was investigated. BM is inherently fluorescent (Figure S6) and has been used previously for bioimaging.[37,38] After 365 nm UV irradiation, the fluorescence decreased due to CB[8]-mediated photodimerization of the BM groups (Figure S7). However, the irradiation of HA-BM and CB[8] using 254 nm UV light, to be used in future aspects of this work for thiol-Nor cross-linking, yielded a limited decrease in absorbance (Figure S5), supporting the stability of the supramolecular BM_2⊂CB[8] ternary complex under these conditions. Indeed, as 254 nm irradiation was shown to reverse photodimer formation,[27] these data further support the limited impact of 254 nm UV light on supramolecular cross-linking.

Supramolecular hydrogels were then prepared by mixing HA-BM with CB[8] at a CB[8]:BM molar ratio of 0.5 and a polymer concentration of 20 mg mL^{-1} HA-BM (7.68 mM BM). Subsequently, 365 nm UV light was applied to convert the supramolecular cross-links into covalent cross-links, as confirmed by oscillatory rheology (Figure 2E). Before UV, the supramolecular hydrogel exhibited frequency-dependent changes in the storage modulus (G'), a behavior typical of supramolecular host−guest hydrogel networks. In addition, a crossover between G' and the loss modulus (G'') was observed at a frequency of ∼0.40 rad s^{-1}, corresponding to a relaxation time of cross-link exchange in the network of ∼16 s. These values for dynamic bond exchange are much slower than those previously observed for a hydrogel prepared from CB[8] cross-linking of BM groups presented on a PEG macromer,[27] suggesting that increased structure and polymer entanglements of the HA backbone acts to slow the apparent cross-link exchange. After UV irradiation, G' was frequency-independent, as is a typical feature of covalent gels. Both hydrogels with and without UV had the same values for G' at a higher frequency, and these remained constant over time (Figure S8A), supporting a consistent network topology before and after the conversion of supramolecular cross-links to their covalent form. UV irradiation did, however, decrease G'' considerably, supporting the existence of a more elastic network. The dynamic network was further confirmed by static mechanical testing through stress relaxation and creep tests. The supramolecular hydrogel showed very fast energy dissipation upon applying 10% strain, while the dimerized hydrogel did not show stress relaxation over time (Figure 2F). Similarly, the hydrogel before UV showed a higher increase in creep compliance over time than the dimerized hydrogel (Figure S8C). In addition, step-strain rheology of the supramolecular hydrogel showed deformation under high strain (200%) and recovery to normal mechanical properties instantly upon a reduction in strain (Figure S8D), supporting shear-thinning and self-healing characteristics for the supramolecular network.

Next, spatial control of the hydrogel dynamics was investigated by 365 nm UV irradiation using a photomask. HA-BM possesses fluorescence with an excitation wavelength of 374 nm and an emission wavelength of 518 nm (Figure S6), which allows imaging using a DAPI filter (blue color) of a microscope. Given that BM fluorescence decreases upon UV irradiation and BM photodimerization, fluorescence microscopy therefore enables direct observation of cross-link state with spatial precision without the need for any supplemental dyes. After UV irradiation through a photomask with 200 μm stripes, the blue stripes were observed (Figure 2G); this blue region is the dynamic supramolecular hydrogel that was masked from UV exposure, while the dark region is the covalent hydrogel region that was cross-linked by UV irradiation and BM photodimerization. Quantification of the fluorescence intensity confirmed the spatial dependence of the blue signal in regions matching the dimensions of the photomask (Figure 2I). A similar result was obtained using a photomask with ∼100 μm stripes, with the resulting hydrogel pattern having stripes of a correspondingly reduced width (Figure 2H,2J). Therefore, the fluorescence of BM groups of the hydrogel enables direct observation of hydrogel cross-linking and, by extension, hydrogel dynamics, which can be controlled at the microscale using UV irradiation with photomasks.

2.4. Spatial Control of Viscoelasticity within Hydrogels. To prepare viscoelastic hydrogels, the supramolecular BM_2⊂CB[8] interaction and thiol-Nor cross-linking were introduced sequentially. It has been reported that thiol-containing compounds can conjugate to the double bond of the polymethine bridge of cyanine dyes.[39−41] However, it was unclear if thiol-containing compounds could react with the BM guest during the thiol-Nor addition under free radical conditions. To confirm the structural integrity of BM groups under conditions of the thiol-Nor reaction, dilute HA-BM in complex with CB[8] and either dithiothreitol (DTT) or a thiol-containing rhodamine dye was exposed to these same free

https://doi.org/10.1021/acsami.3c12514
ACS Appl. Mater. Interfaces 2023, 15, 58181−58195

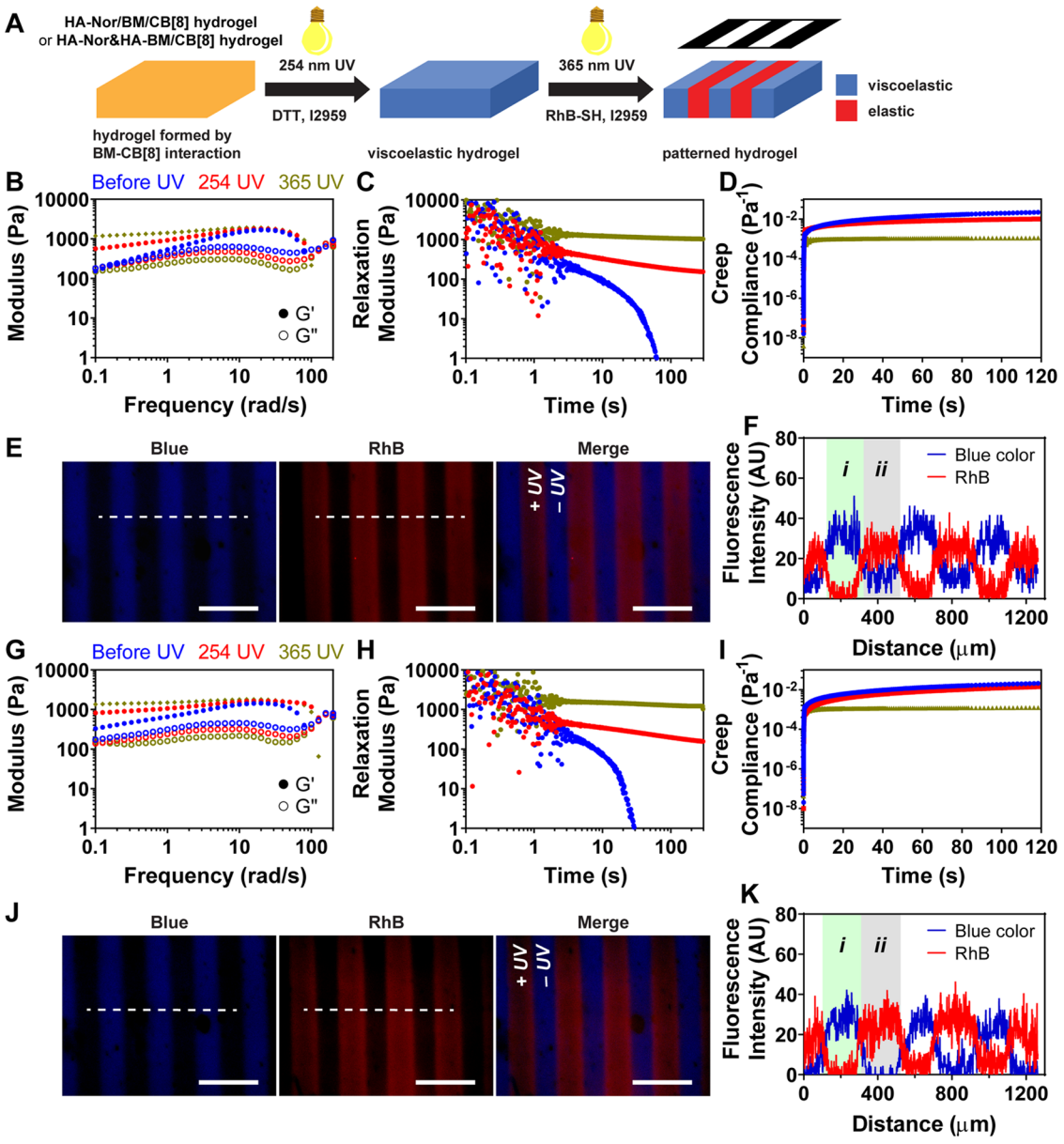

Figure 3. UV light-controlled viscoelasticity of hydrogels, HA-Nor/BM with CB[8] and HA-Nor and HA-BM with CB[8], prepared by BM_2⊂CB[8] interaction and thiol-Nor covalent cross-linking. (A) Scheme of photopatterning hydrogels with thiol-containing rhodamine B (Rh-SH) molecules using a photomask. (B) Frequency sweep (2% strain), (C) stress relaxation (10% strain), and (D) creep (100 Pa stress) rheology for the hydrogel of HA-Nor/BM with CB[8] before UV (blue), after 254 nm UV (red) irradiation in the presence of DTT/I2959, and 365 nm UV (olive) irradiation. (E) Photopatterning of hydrogel of HA-Nor/BM with CB[8] using a photomask with 200 μm stripes. The patterns were imaged by DAPI (blue), fluorescein isothiocyanate (FITC) (green), and Texas Red (red) microscope filters, with fluorescence intensities quantified along the dashed white line (F). (G) Frequency sweep (2% strain), (H) stress relaxation (10% strain), and (I) creep (100 Pa stress) rheology of hydrogel prepared from HA-Nor and HA-BM with CB[8] before UV (blue), after 254 nm UV (red) irradiation in the presence of DTT/I2959, and 365 nm UV (olive) irradiation. (J) Photopatterning of hydrogel prepared from HA-Nor and HA-BM with CB[8] using a photomask with 200 μm stripes. The patterns were imaged by DAPI (blue), FITC (green), and Texas Red (red) microscope filters, with fluorescence intensities quantified along the dashed white line (K). (i) viscoelastic hydrogel region; (ii) elastic hydrogel region. Scale bars: 500 μm.

radical conditions activated by 254 nm UV light. The NMR spectra of the HA-BM and CB[8] complex after reacting with DTT showed identical signals to the original complex (Figure S4A), and no rhodamine signal was found after the reaction (Figure S4B,C). The results indicate that HA-BM in the presence of CB[8] cannot react with thiol-containing molecules under free radical conditions, and the HA-BM and CB[8] complex remains unaltered under these conditions and is available for subsequent dimerization using higher wavelength UV light.

The native ECM is heterogeneous and undergoes dynamic changes in mechanical properties throughout different cellular processes. Dynamic hydrogels with controlled and tunable viscoelasticity offer one route to mimic the dynamic features of the ECM.[42−44] UV light provides a straightforward and minimally disruptive way to tune viscoelasticity,[45] though the use of this approach typically requires additional chemical reagents to facilitate secondary reactions. With the hydrogel having both BM_2⊂CB[8] interactions and thiol-Nor cross-linking, viscoelasticity could be tuned using locally applied UV

https://doi.org/10.1021/acsami.3c12514
ACS Appl. Mater. Interfaces 2023, 15, 58181−58195

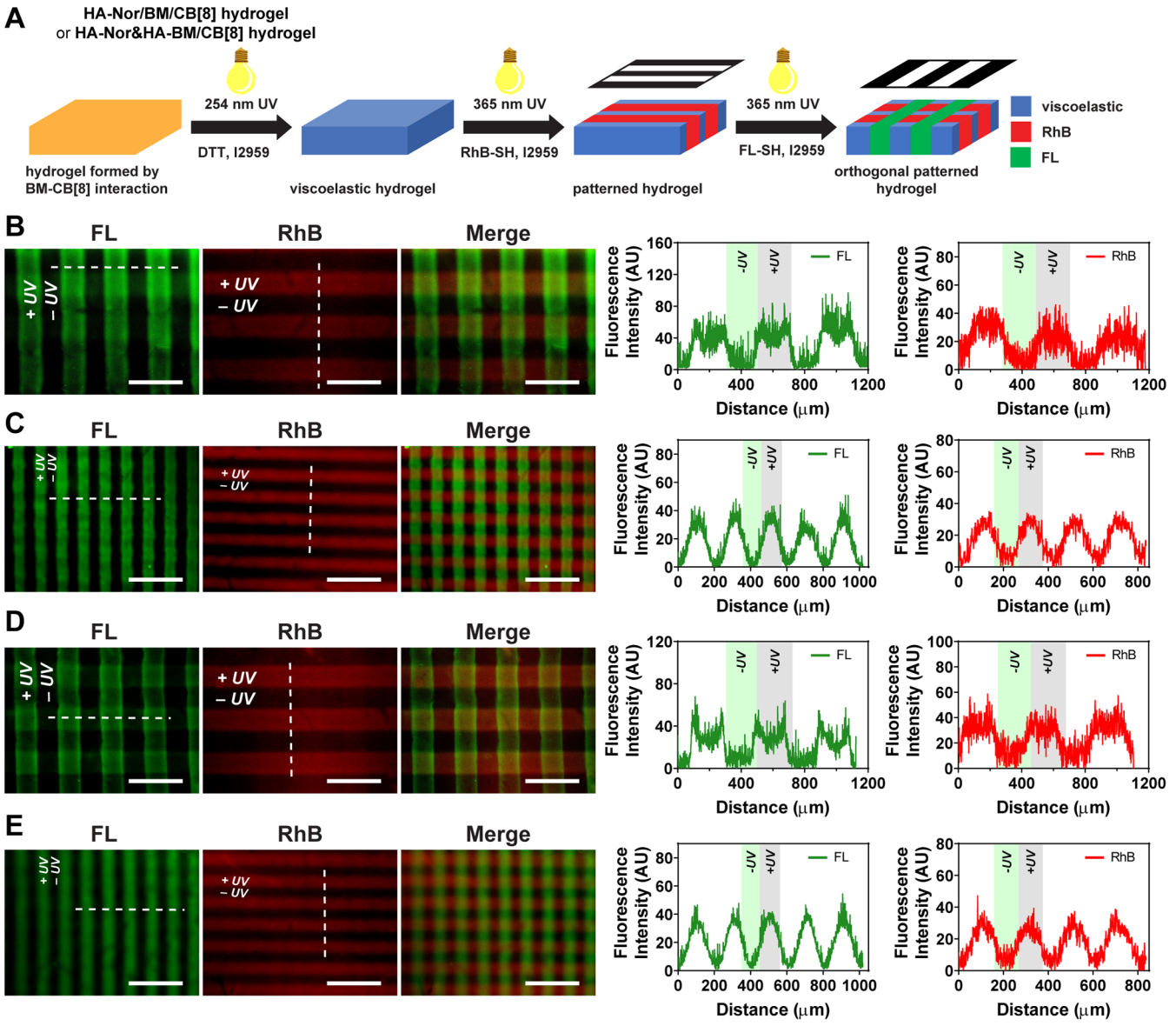

Figure 4. Orthogonal photopatterning hydrogels of HA-Nor/BM with CB[8] and HA-Nor and HA-BM with CB[8]. (A) Schematic of orthogonal photopatterning of hydrogels with thiol-containing rhodamine B (RhB-SH) and thiol-containing fluorescein (FL-SH) molecules. Orthogonal photopatterning a hydrogel of HA-Nor/BM with CB[8] using photomasks of (B) 200 μm or (C) 100 μm stripes. The patterns were imaged by FITC (green) and Texas Red (red) microscope filters, with fluorescence intensities quantified along the dashed white line. Orthogonal photopatterning hydrogels of HA-Nor and HA-BM with CB[8] using photomasks of (D) 200 μm or (E) 100 μm stripes. The patterns were imaged by FITC (green) and Texas Red (red) microscope filters, with fluorescence intensities quantified along the dashed white line. Scale bars: 500 μm.

light to promote BM dimerization and conversion of supramolecular to covalent cross-linking without the need for additional chemical reagents.

The supramolecular hydrogel without covalent cross-linking was obtained after mixing HA-Nor/BM with CB[8] at 20 mg mL^{-1} (7.53 mM BM). Upon 254 nm UV (10 mW cm^{-2} for 20 min) irradiation, thiol-Nor cross-linking was introduced to generate a dual-cross-linked viscoelastic hydrogel with both supramolecular BM_2⊂CB[8] cross-links and covalent thiol-Nor cross-links. Subsequent 365 nm UV (10 mW cm^{-2} for 1 h) irradiation could then activate BM photodimerization to form an elastic hydrogel with only covalent cross-links. The change in mechanical properties was confirmed by oscillatory rheology; a decrease in the loss modulus (G'') after UV irradiation with both 254 nm UV as well as 365 nm light marked this transition of the cross-links (Figure S9A). The dual-cross-linked hydrogel with supramolecular BM_2⊂CB[8] cross-links showed a frequency-dependent modulus consistent with its viscoelastic character, whereas the elastic hydrogel resulting following BM photodimerization was frequency-independent (Figure 3B). Notably, the viscoelastic hydrogel exhibited stress relaxation behavior that was slower than that of the hydrogel formed from only supramolecular interactions; the elastic hydrogel did not show stress relaxation (Figure 3C). Furthermore, the viscoelastic hydrogel showed a significantly higher creep than the elastic hydrogel (Figure 3D). Structural deformation and recovery using step-strain rheology supported the viscoelastic hydrogels to have dynamic and self-healing properties (Figure S9C,D). Therefore, UV irradiation offered a facile means to control the bulk mechanical properties of these dual-cross-linked hydrogels due to the supramolecular-to-

https://doi.org/10.1021/acsami.3c12514
ACS Appl. Mater. Interfaces 2023, 15, 58181−58195

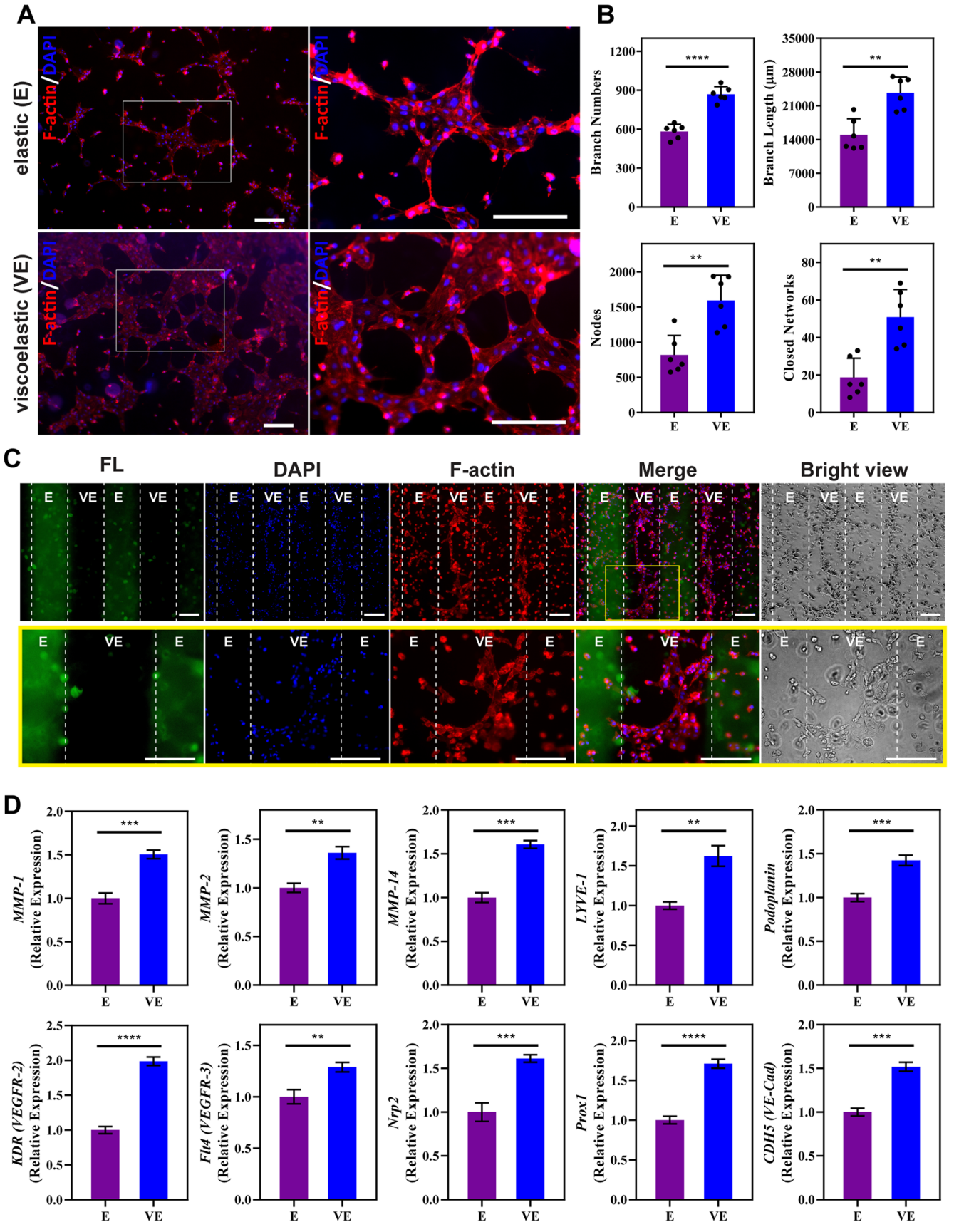

Figure 5. Impact of Substrate Viscoelasticity on Cellular Response. (A) Representative images of lymphatic endothelial cells (LECs) on elastic (E) and viscoelastic (VE) hydrogels after culture for 6 h with 100 ng mL^{-1} VEGF-C, 50 ng mL^{-1} bFGF, and 1.5 μM S1P. Scale bars: 200 μm. (B) Quantification of lymphatic tube formation. Increased branches, nodes, and closed networks were observed for culture on VE hydrogels. Data represents the mean ± standard deviation (SD) of 6 biological replicates performed. (C) Representative images of LECs on hydrogels

https://doi.org/10.1021/acsami.3c12514
ACS Appl. Mater. Interfaces 2023, 15, 58181−58195

Figure 5. continued

photopatterned with 400 μm stripes after incubation for 12 h with 100 ng mL^{-1} VEGF-C, 50 ng mL^{-1} bFGF, and 1.5 μM S1P. Stripes labeled with fluorescein (FL) showed the region of the E hydrogel. The lower panel is an enlarged view of the region within the yellow square. Cell alignment was evident on VE stripes corresponding to the direction of the stripe, along with connected branches. Scale bars: 200 μm. (D) LEC gene expression for *MMP-1*, *MMP-2*, *MMP-14*, *LYVE-1*, *Podoplanin*, *KDR (VEGFR2)*, *Flt4 (VEGFR3)*, *Neuropilin-2 (Nrp2)*, *Prox1*, and *CDH5* (*VE-Cad*) after culture on E and VE hydrogels for 12 h with 100 ng mL^{-1} VEGF-C, 50 ng mL^{-1} bFGF, and 1.5 μM S1P. Values shown are means ± SD from 3 independent experiments performed with real-time qRT-PCR with triplicate readings. A two-tailed unpaired *t*-test was performed on the data. $^{**}p < 0.01$; $^{***}p < 0.001$; $^{****}p < 0.0001$.

covalent nature of the BM $_2$⊂CB[8] homoternary cross-linking.

The ability to tune the viscoelasticity at the microscale was investigated by photopatterning using UV light with a photomask. The thiol-Nor chemistry incorporated into the hydrogels enabled visualization of photopatterning using the thiol-containing fluorescein (FL-SH) fluorophore (Figure S10). The innate blue fluorescence of BM groups in the hydrogel coupled with a red-emissive thiol-containing rhodamine B (RhB-SH) enabled a complementary way to visualize these patterns (Figure 3A). As 365 nm UV activates both BM photodimerization and the thiol-Nor reaction, it was expected that regions exposed to UV would have red fluorescence only, while regions without UV exposure would have blue fluorescence. The viscoelastic hydrogel prepared from HA-Nor/BM with CB[8] (254 nm UV 10 mW cm^{-2} for 5 min) was photopatterned through a photomask of 200 μm stripes with 365 nm UV (10 mW cm^{-2} for 2 min) in the presence of RhB-SH. After washing away free RhB-SH, the hydrogel had disparate regions of blue fluorescence and red fluorescence (Figure 3E,F). Based on the material design here, the red stripes mark the elastic network with photodimerized BM cross-links, while the blue stripes denote the viscoelastic region with intact dynamic supramolecular cross-linking. Photopatterning using a photomask with 100 μm stripes achieved comparable results of the expected reduction in pattern dimensions (Figure S11).

Next, control of viscoelasticity was expanded to the double-network hydrogel prepared from the HA-Nor and HA-BM polymers combined with dithiol and CB[8]. The hydrogels prepared with only supramolecular cross-linking (no UV) and activated thiol-Nor covalent cross-linking (254 nm UV) had frequency-dependent behavior (Figure 3G) and cyclic shear-induced flow and recovery (Figure S12C,D). The viscoelastic character was further confirmed by stress relaxation (Figure 3H) and creep compliance (Figure 3I). The hydrogel prepared with all covalent cross-linking (365 nm UV) had a frequency-independent character, no stress relaxation, and limited creep behavior. The hydrogels showed relatively weaker mechanical strength, which could be attributed to the lower DS value of Nor and BM on HA. Using modified HA polymers with higher DS of Nor and BM and preparing hydrogels at higher concentrations may facilitate improving the mechanical strength. Spatial control of viscoelasticity using photopatterning enabled alternating blue and red fluorescence marking viscoelastic and elastic stripes, respectively (Figures 3J,K and S13). The stress relaxation behavior and spatial control by UV light in the double-network hydrogel were similar to that in the dual-cross-linked hydrogel. The results indicate precise spatial control of viscoelasticity by UV light without additional chemical reagents for secondary cross-linking. Moreover, in addition to tuning viscoelasticity by photopatterning, the inclusion of Nor groups allows the patterning of biochemical cues through the inclusion of thiol-containing biomolecules.

2.5. Orthogonal Photopatterning of Viscoelastic Hydrogels. After demonstrating spatial control of viscoelasticity using UV without the need for added chemical reagents for secondary cross-linking, the capability to incorporate microenvironmental features for cell culture was investigated through orthogonal photopatterning of dyes used as model biomolecules. The dual-cross-linked viscoelastic hydrogel prepared from HA-Nor/BM and CB[8] was first incubated with RhB-SH and photopatterned using 365 nm UV light with a photomask. After removing free RhB-SH, the hydrogel was then incubated with FL-SH and further photopatterned with a photomask placed at 90° angle relative to the initial photomask (Figure 4A). A mask with a 200 μm stripe pattern yielded a cross-hatched pattern of stripes of these sample dimensions at a 90° angle (Figure 4B). The green/red stripes depict the elastic hydrogel modified with both dyes, while the dark stripes were viscoelastic hydrogels without either modification. The 100 μm mask generated hydrogels with narrower cross-hatched stripes, also matching the dimensions of the mask (Figure 4C). Orthogonal photopatterning was likewise applied to double-network hydrogels prepared from HA-Nor and HA-BM with CB[8]. Cross-hatched stripes of ∼200 μm (Figure 4D) and ∼100 μm (Figure 4E) width were also demonstrated by both imaging and fluorescence intensity quantification. The viscoelastic hydrogel thus offered a flexible approach to pattern multiple biomolecules and thereby achieve simultaneous spatial control over both molecular functionalization and viscoelasticity through the sequential application of different photomask patterns. Therefore, both biochemical cues and viscoelasticity can be combined with the hydrogel to study the cell behavior, such as screening microenvironmental parameters.[30]

2.6. Viscoelastic Hydrogels Promote the Formation of Lymphatic Cord-like Structures. Mechanical cues are important in regulating the function of endothelial cells during vascular and lymphatic development.[46−49] Dynamic mechanical properties, such as the shear stress induced by fluid flow, have inspired the design of dynamic hydrogels for engineering vascular and lymphatic tissues.[50−53] ECM with softer mechanics has been shown to enhance lymphatic vessel formation by inducing a globin transcription factor binding protein 2 (GATA2) dependent transcriptional program.[54] We previously showed a covalently cross-linked HA hydrogel with matrix stiffness priming lymphatic CLS formation directed by vascular endothelial growth factor-C (VEGF-C).[46] However, little is known about the mechanosensing cues of ECM viscoelasticity on the LEC behavior. Here, the response of LECs to viscoelasticity was studied with the viscoelastic supramolecular hydrogels prepared from 7 mg mL^{-1} HA-Nor/BM (2.63 mM BM). The BM and Nor modifications on HA hydrogels did not induce cell death in the course of culturing

https://doi.org/10.1021/acsami.3c12514
ACS Appl. Mater. Interfaces 2023, 15, 58181−58195

LECs on hydrogels for 3 days (Figure S14). As there are no cell anchoring sites on the modified HA hydrogels, RGD peptides were supplemented during hydrogel preparation, enabling LECs to attach and spread; LECs had a rounded morphology on hydrogels without RGD modification (Figure S15).

To promote lymphatic CLS formation, LECs were cultured on RGD-modified hydrogels in media supplemented with VEGF-C, basic fibroblast growth factor (bFGF), and sphingosine 1-phosphate (S1P).[47,55,56] After incubation for 6 h, more closed networks with a higher extent of branching were observed on viscoelastic hydrogels than on elastic hydrogels (Figure 5A). Lymphatic tube formation was quantified by the kinetic analysis of vasculogenesis (KAV) Fiji plug-in. Quantification revealed that the dynamic viscoelastic network induced more branches and greater total branch length than the static elastic hydrogels (Figure 5B). Similarly, the viscoelastic hydrogel exhibited a greater number of nodes and closed networks. Furthermore, viscoelastic hydrogels showed relatively increased focal adhesion kinase (FAK) expression and F-actin density and alignment (Figure S16), which imply enhanced cell spreading and migration through enhancing focal adhesion assembly and increasing F-actin stress fiber in response to viscoelasticity. Overall, these results showed that viscoelastic hydrogels provide the mechanical dynamics needed to support lymphatic CLS formation.

To spatially control LECs during CLS formation, photopatterned hydrogels were next explored. Given the size of lymphatic CLS formed on hydrogels,[46] a photomask with 400 μm stripes was utilized for photopatterning prior to LEC culture (Figure 5C). After 12 h of incubation, LECs were observed to align along the viscoelastic stripe; LECs on the elastic stripes showed scattered morphology (Figure 5C, top row). On the viscoelastic stripes, semicircle-like branched structures were observed, supporting a tendency to form branched and closed networks (Figure 5C, bottom row). It should be noted that the coordination of a relatively large area of cells is required to form closed networks, and, as such, while branched structures were observed, no closed networks were identified on the viscoelastic stripes. Overall, these observations suggest that photopatterning of viscoelastic regions enables spatial control of lymphatic CLS formation.

To further investigate the impact of viscoelasticity on lymphatic tube formation, qRT-PCR was performed to compare the gene expression of LEC characteristic markers on both elastic and viscoelastic hydrogels (Figure 5D). Since 6 h was determined to be the ideal endpoint for lymphatic CLS formation, 12 h was selected as the endpoint for gene expression analysis to ensure that the signaling cascade in response to elastic and viscoelastic hydrogels can be fully captured.[46,58] After culturing human LECs for 12 h, viscoelastic hydrogels showed increased expression of lymphatic vessel endothelial hyaluronan receptor-1 (*LYVE-1*), *podoplanin*, and prospero homeobox 1 (*Prox1*) compared to LECs cultured on elastic hydrogels; all three genes are key lymphatic markers. As a homologue to the CD44 glycoprotein, LYVE-1 is used by LECs to interact with HA.[46,59] Podoplanin is the only known endogenous ligand for C-type lectin-like receptor-2 (CLEC-2), which is important for blood and lymphatic separation during embryonic development.[60−63] The transcription factor *Prox1* is the master regulator of lymphatic phenotypes and vasculatures.[64,65] Therefore, elevated expression of key lymphatic markers *LYVE-1*, *podoplanin*, and *Prox1* suggests that viscoelastic hydrogels preserve the LEC phenotype, an important factor in enabling lymphatic CLS formation. Similarly, the expression of vascular endothelial growth factor receptor-2 (*VEGFR2*), *VEGFR3*, and Neuropilin-2 (*Nrp2*) increased on viscoelastic hydrogels. *Nrp2* functions to augment the signaling of VEGF-C to *VEGFR2* and *VEGFR3*, which promotes the survival and migration of LECs.[66,67] Thus, an enhanced ability of LECs to respond to VEGF-C stimulation when cultured on viscoelastic hydrogels likely drives enhanced lymphatic CLS formation.[46,67] Furthermore, lymphatic CLS formation entails cell migration to form cellular junctions. The results also showed an increased expression of MMPs, including *MMP-1*, *MMP-2*, and *MMP-14*, when LECs were cultured on viscoelastic hydrogels. Higher MMP expression can promote the degradation and remodeling of the extracellular matrix, thus directing lymphatic tube formation.[46,47] LECs cultured on viscoelastic hydrogels also expressed higher expression of VE-Cad (*CDH5*), an endothelial-specific adhesion molecule that mediates intercellular conjunction and lymphatic maintenance.[68−70] Altogether, these data suggest that viscoelastic hydrogels support lymphatic phenotypes and promote lymphatic CLS formation.

3. CONCLUSIONS

In conclusion, HA-based hydrogels were designed with spatially controlled and UV-directed tuning of viscoelasticity by combining supramolecular and covalent cross-linking interactions to mimic the dynamic and spatially heterogeneous properties of the native ECM. The cucurbit[8]uril (CB[8]) macrocycle affords supramolecular cross-linking by the formation of a ternary complex with pendant *trans*-Brooker's Merocyanine (BM) guests. CB[8] then catalyzes the photodimerization of BM guests within its portal under UV irradiation, enabling a user-directed means of controlling hydrogel dynamics by using orthogonal photopatterning with photomasks. This approach enables external and spatially resolved control of network dynamics without the need for additional chemical reagents to change cross-linking. The mechanical strength of the hydrogels needs to be further improved to accommodate specific biological applications. We demonstrate that these dynamic hydrogels can provide spatially controlled substrates for the culture of human LECs to direct lymphatic CLS formation. The presentation of HA to the surface of LECs has been shown to preserve the lymphatic phenotypes.[71] Modulating the viscoelastic properties of the HA hydrogels can further promote lymphatic CLS formation by enhanced expression of key lymphatic markers, such as *LYVE-1*, *podoplanin*, and *Prox1*, along with expression of *Nrp2*, *VEGFR2*, and *VEGFR3* to enhance VEGF-C stimulation. Whereas previous studies have shown the importance of matrix stiffness for lymphatic tube formation,[46,54] this report offers evidence supporting a role for matrix viscoelasticity in promoting lymphatic development and lymphatic CLS formation. Promising results from this current work warrant future studies to investigate the effects of viscoelastic hydrogels on lymphatic formation *in vivo*. Collectively, insights gained from this study can be used to design viscoelastic hydrogels for future study of basic lymphatic biology, as well as toward various approaches in tissue engineering applications.

https://doi.org/10.1021/acsami.3c12514
ACS Appl. Mater. Interfaces 2023, 15, 58181−58195

4. EXPERIMENTAL SECTION

4.1. Materials. Sodium hyaluronic acid (HA) with a molecular weight of 73 kDa was purchased from Lifecore Biomedical. Propargylamine (98%), dithiothreitol (DTT, 98%), 2-hydroxy-4′-(2-hydroxyethoxy)-2-methylpropiophenone (I2959, 98%), *N*,*N*-dimethylformamide (DMF, 99.8%), copper(II) sulfate pentahydrate (98%), (+)-sodium L-ascorbate (99%), 2-(*N*-morpholino)-ethanesulfonic acid (MES, 99%), deuterium oxide (D_2O, 99.9%), and triethanolamine (99%) were purchased from Sigma-Aldrich and used without further purification. 5-Norbornene-2-methylamine (mixture of isomers, 98%) and 4-(4,6-dimethoxy-1,3,5-triazin-2-yl)-4-methylmorpholinium chloride (DMTMM, 98%) were purchased from TCI and used without further purification. Tris(3-hydroxypropyltriazolylmethyl)amine (THPTA, 95%) was purchased from Click Chemistry Tools. Z-rhodamine-SH (RhB-SH, 95%) was purchased from Kerafast. Fluorescein-containing peptide FL-DDDCG (FL-SH, 95%) was purchased from Genscript. Other chemical reagents were purchased from VWR. Cucurbit[8]uril (CB[8]) was synthesized as previously reported. Deionized water (DI H_2O) with a resistivity of 18 MΩ cm^{-1} was used as a solvent for dialysis experiments, and dialysis was performed using cellulose membranes with a molecular weight cutoff of 7 kDa. Photomasks were purchased from CAD/Art Services. An Omnicure S1500 UV light source filtered to 320−390 nm was used for 365 nm UV irradiation. A Rayonet RPR-200 photoreactor (Southern New England Ultraviolet) equipped with a circumferential arrangement of 16 lamps (254 nm) was used for 254 nm UV irradiation. The absorbance and fluorescence spectra were collected with a Spark Microplate Reader (Tecan).

4.2. Nuclear Magnetic Resonance (NMR) Spectra. ^{1}H NMR spectra were recorded on a Bruker AVANCE III HD 400 (400 MHz) or 500 spectrometers (500 MHz). The chemical shifts of all NMR spectra were reported in delta (δ) units and expressed as parts per million (ppm).

4.3. Synthesis of BM-Azide. 4-Picoline (4.86 mL, 50 mmol) and 1,6-dibromohexane (38.4 mL, 200 mmol) were mixed in a round-bottom flask with 100 mL of acetonitrile. After refluxing at 90 °C overnight, the mixture was cooled to room temperature. The solvent was removed by rotovap, and then diethyl ether was added. The solid was collected and then recrystallized in ethanol. Compound **1** was obtained as a white solid. ^{1}H NMR (400 MHz Bruker, 25 °C, $CDCl_3$, Figure S17): δ (ppm) = 9.41−9.40 (d, 2H), 7.87−7.85 (d, 2H), 4.98−4.94 (t, 2H), 3.40−3.36 (t, 2H), 2.66 (s, 1H), 2.08−2.00 (m, 2H), 1.86−1.79 (m, 2H), 1.51−1.47 (m, 4H).

Compound **1** (300 mg, 0.89 mmol) was dissolved in 20 mL of acetonitrile. Sodium azide (578 mg, 8.9 mmol) was then slowly added to the solution. The mixture was refluxed at 90 °C overnight. The solvent was removed, and then the residue was redissolved in dichloromethane. The liquid phase was collected. Compound **2** was obtained as a white powder after solvent removal. ^{1}H NMR (400 MHz Bruker, 25 °C, $CDCl_3$, Figure S18): δ (ppm) = 9.38−9.37 (d, 2H), 7.86−7.85 (d, 2H), 4.99−4.96 (t, 2H), 3.27−3.24 (t, 2H), 2.67 (s, 1H), 2.05−2.00 (m, 2H), 1.58−1.57 (m, 2H), 1.56−1.43 (m, 4H).

Compound **2** (267 mg, 0.896 mmol) and 4-hydroxybenzaldehyde (131 mg, 1.08 mmol) were dissolved in 10 mL of isopropyl alcohol. Eight drops of piperidine were added to the solution. The mixture was stirred at 70 °C overnight. After cooling to room temperature, the precipitate was collected. The BM-azide product was obtained as a purple powder. ^{1}H NMR (400 MHz Bruker, 25 °C, D_2O, Figure S19): δ (ppm) = 8.48−8.47 (d, 2H), 7.91−7.89 (d, 2H), 7.72−7.68 (d, 1H), 7.59−7.57 (d, 2H), 7.11−7.06 (d, 1H), 6.86−6.84 (d, 2H), 4.42−4.38 (m, 2H), 3.29−3.26 (m, 2H), 1.99−1.91 (m, 2H), 1.59−1.52 (m, 2H), 1.42−1.38 (m, 2H).

4.4. Synthesis of HA-Norbornene (HA-Nor). HA (200 mg) was dissolved in MES buffer (20 mL, 0.1 M, pH 5.5). To improve the solubility of small molecules and enhance reaction efficiency, ethanol (6.67 mL) was added to the solution. DMTMM (551.6 mg, 4 equiv relative to the COOH groups on the HA) was added and stirred at room temperature for 30 min. 5-Norbornene-2-methylamine (61.5 μL, 1 equiv) was mixed with MES buffer (pH 5.0) (v/v, 1/1) and then added to the solution. The mixture was stirred at room temperature for 4 h. Subsequently, the reaction mixture was dialyzed against 1% NaCl solution for 2 days and DI H_2O for 2 days. The solution was lyophilized and stored at −20 °C. The degree of substitution of Nor was calculated on the basis of disaccharide repeating units by ^{1}H NMR integration.

4.5. Synthesis of Alkynylated HA (HA-Alkyne). HA (300 mg) was dissolved in MES buffer (30 mL, 0.1 M, pH 5.5), followed by the addition of ethanol (10 mL). DMTMM (206.9 mg, 1 equiv on the basis of COOH groups on HA) was added, and the mixture was stirred at room temperature for 30 min. Propargylamine (9.6 μL, 0.2 equiv for 18% HA-alkyne; 19.2 μL, 0.4 equiv for 30% HA-alkyne) was mixed with MES buffer (pH 5.0) (v/v, 1/1) and then added to the solution. The mixture was stirred at room temperature for 24 h. Subsequently, the reaction mixture was dialyzed against 1% NaCl solution for 2 days and DI H_2O for 2 days. The solution was lyophilized and stored at −20 °C. The degree of substitution of the alkyne was calculated on the basis of disaccharide repeating units by ^{1}H NMR integration.

4.6. Synthesis of HA-Nor/Alkyne. HA (300 mg) was dissolved in MES buffer (30 mL, 0.1 M, pH 5.5), followed by the addition of ethanol (10 mL). DMTMM (413.7 mg, 2 equiv on the basis of the COOH groups on the HA) was added and stirred at room temperature for 30 min. The desired amounts of 5-norbornene-2-methylamine and propargylamine were mixed with MES buffer (pH 5.0, v/v, 1/1) and then added to the solution. HA-Nor/alkyne with modification ratios of 8% Nor-18% alkyne, 20% Nor-18% alkyne, 18% Nor-22% alkyne, 15% Nor-30% alkyne, 30% Nor-10% alkyne, and 38% Nor-12% alkyne were achieved by feed ratios of 0.2 equiv Nor-0.2 equiv alkyne, 0.7 equiv Nor-0.2 equiv alkyne, 0.6 equiv Nor-0.25 equiv alkyne, 0.4 equiv Nor-0.4 equiv alkyne, 1.2 equiv Nor-0.12 equiv alkyne, and 2 equiv Nor-0.2 equiv alkyne were added, respectively. The mixture was stirred at room temperature for 21 h. Subsequently, the reaction mixture was dialyzed against 1% NaCl solution for 2 days and DI H_2O for 2 days. The solution was lyophilized and stored at −20 °C. The degree of substitution of Nor and alkyne was calculated on the basis of disaccharide repeating units determined by ^{1}H NMR integration.

4.7. Synthesis of HA-BM or HA-Nor/BM. In a 50 mL round-bottomed vessel, HA-alkyne or HA-Nor/alkyne (140 mg) was dissolved in MES buffer (14 mL, pH 5.5), followed by the addition of ethanol (4.67 mL). BM-azide in DMF (1.3 equiv, 50 mg mL^{-1}, based on alkyne) was added. THPTA (0.2 equiv, based on alkyne) was mixed with a freshly prepared $CuSO_4{\cdot}5H_2O$ solution (0.4 equiv, 20 mg mL^{-1}, based on alkyne) in MES buffer (pH 5.5) and added to the reaction solution. The reaction mixture was placed under a flow of nitrogen gas, and freshly prepared Na-ascorbate solution (1.2 equiv, 50 mg mL^{-1}, based on alkyne) in MES buffer (pH 5.5) was added to the mixture. The mixture was covered with aluminum foil and stirred at room temperature for 24 h. Subsequently, the reaction mixture was dialyzed against 1% NaCl solution for 2 days and DI H_2O for 3 days. The solution was lyophilized and stored at −20 °C. The products were characterized by ^{1}H NMR spectroscopy.

4.8. Supramolecular Interaction between HA-BM and CB[8]. The stock solution of HA-BM was prepared by dissolving it in DI H_2O at a concentration of 5 mg mL^{-1}. A series volume of CB[8] stock solutions at 8 mg mL^{-1} in DI H_2O was added to obtain the desired molar ratio of CB[8] to BM, and extra DI H_2O was added to reach a final concentration of 0.5 mg mL^{-1} for HA-BM. After incubating at room temperature for 30 min, the solutions were transferred to a microplate, and absorbance scanning was performed between 200 and 600 nm. The ratios of absorbance at 396 to 374 nm were calculated and plotted vs the molar ratio of CB[8].

4.9. Photodimerization of HA-BM by UV Irradiation. HA-BM was mixed with CB[8] (CB[8]:BM molar ratio 0.5) at a polymer concentration of 0.5 mg mL^{-1} in DI H_2O to prepare homoternary cross-linked polymer solutions. The HA-BM and CB[8] complexes were irradiated with 365 nm UV (10 mW cm^{-2}) or 254 nm UV for various times. Fluorescence emission scanning (excitation wavelength 378 nm) and absorbance scanning from 200 to 600 nm were

https://doi.org/10.1021/acsami.3c12514
ACS Appl. Mater. Interfaces 2023, 15, 58181−58195

performed, and the absorbance at 378 nm was plotted against exposure time. The data was fit to a standard first-order reaction rate equation to obtain the rate constant and reaction half-life. For comparison, the polymer solution of HA-BM at the same concentration without CB[8] was also subjected to the same UV irradiation protocol.

To confirm the stability of the HA-BM and CB[8] complex under free radical reaction conditions and ensure no BM reactivity with thiols, 5 mg mL^{-1} HA-BM with CB[8] in DI H_2O was prepared and reacted with DTT and I2959 under exposure to 254 nm UV irradiation. Subsequently, the reaction mixture was dialyzed against 1% NaCl solution for 2 days and DI H_2O for 3 d. The product was characterized by ^1H NMR spectroscopy. In addition, 5 mg mL^{-1} HA-BM with CB[8] was reacted with RhB-SH and I2959 with 254 nm UV irradiation. The reaction mixture was dialyzed against 1% NaCl solution for 2 days and DI H_2O for 3 days. The solution was lyophilized, and the product was characterized by fluorescence emission scanning (excitation wavelength 562 nm) and absorbance scanning from 300 to 700 nm.

4.10. Rheological Characterization. The mechanical properties of the hydrogels were studied by oscillatory rheology on a TA Instruments Discovery HR-2 rheometer. All measurements were performed at 25 °C by using an 8 mm parallel plate geometry, and the gap between the upper plate and Peltier base was sealed with silicone oil to minimize evaporation. Strain sweep measurements from 0.1 to 300% were conducted at 10 rad s^{-1} frequency to determine the linear viscoelastic region. Frequency sweep measurements from 0.1 to 200 rad s^{-1} were then conducted at 2% strain, which was within the linear viscoelastic region. Time sweep measurements over 5 min at 2% strain and 10 rad s^{-1} were conducted to determine storage modulus (G') and loss modulus (G''). The viscoelastic properties of hydrogels were studied by stress relaxation over 5 min following the application of 10% strain and creep tests over 2 min at a constant 100 Pa stress loading. Step-strain experiments were performed at 10 rad s^{-1} by alternating between 2% strain for 60 s and 200% strain for 30 s for three cycles.

4.11. Hydrogel Preparation and Tuning of Viscoelasticity. All hydrogels were prepared with DI H_2O as the solvent at a polymer concentration of 20 mg mL^{-1}. The molar ratio of CB[8] to the BM groups was 0.5. For hydrogels from HA-Nor/BM with CB[8] and HA-Nor and HA-BM with CB[8], DTT at a molar ratio of 0.5 to Nor groups and 0.5 mg mL^{-1} I2959 photoinitiator were added for thiol-Nor cross-linking. The viscoelasticity of hydrogels was tuned by UV irradiation with 254 nm UV (10 mW cm^{-2}) for 20 min to introduce thiol-Nor covalent cross-linking and 365 nm UV (10 mW cm^{-2}) for 1 h to induce photodimerization of the BM_2⊂CB[8] homoternary complex.

4.12. Photopatterning Hydrogels. Thin hydrogels of ∼1 mm thickness were prepared in a 4 × 4 × 1 mm poly(dimethylsiloxane) (PDMS) mold for photopatterning. For the hydrogel of HA-BM with CB[8], photomasks of 200 or 100 μm stripes were placed atop and irradiated using 365 nm UV (10 mW cm^{-2}) for 2 min. The patterned hydrogel was imaged with DAPI and using an inverted Echo Revolve microscope. For the HA-Nor hydrogel, the hydrogel was swelled in an FL-SH (0.1 mM) solution containing 0.5 mg mL^{-1} I2959 at room temperature for 5 min. Subsequently, the hydrogel was irradiated with 365 nm UV (10 mW cm^{-2}) through 200 μm strips for 1 min. The patterned hydrogel was washed with DI H_2O several times prior to imaging with the FITC filter of an Echo Revolve microscope. For spatial control of viscoelasticity within hydrogels, hydrogels containing DTT (0.35 equiv to Nor) and 0.5 mg mL^{-1} I2959 were prepared using the BM_2⊂CB[8] interaction in a 4 × 4 × 1 mm PDMS mold before 254 nm UV (10 mW cm^{-2}) irradiation for 5 min. The PDMS mold was removed, and the hydrogels were swelled in DI H_2O for 15 min. An 8 × 8 × 1 mm PDMS mold was placed around the hydrogels before incubating with the RhB-SH (0.42 μM) solution containing 0.5 mg mL^{-1} I2959 at room temperature for 5 min. Subsequently, hydrogels were irradiated with 365 nm UV (10 mW cm^{-2}) through a photomask with 200 or 100 μm stripes for 2 min. The patterned hydrogels were washed with DI H_2O several times prior to imaging with DAPI and Texas Red filters on an Echo Revolve microscope. For orthogonal photopatterning, hydrogels were incubated with an FL-SH (0.1 mM) solution containing 0.5 mg mL^{-1} I2959 for 5 min after RhB-SH photopatterning. Subsequently, hydrogels were irradiated with 365 nm UV (10 mW cm^{-2}) for 30 s through photomasks of 200 or 100 μm stripes placed at a 90° angle from the initial photomask. The patterned hydrogels were washed with DI H_2O several times prior to imaging with FITC and Texas Red filters of an Echo Revolve microscope.

4.13. Human LEC Culture. Human LECs derived from the dermis of two adult donors (PromoCell, Heidelberg, Germany) were expanded and used for experiments between passages 5 and 9. Human LECs were grown in endothelial growth medium MV2 (EGM MV2; PromoCell) and incubated at 37 °C with 5% CO_2. Human LECs were characterized for the positive expression of CD31, LYVE-1, Prox1, and podoplanin throughout the experiments.[46,60] All cell lines were routinely tested for mycoplasma contamination and were negative throughout this study. Viable cells were visualized by staining the cell membrane with 2 μM calcein AM dye for 20 min at room temperature. Dead cells were determined by staining with 4 μM ethidium homodimer-1 (Invitrogen, L3224) for 30 min at room temperature.

4.14. Lymphangiogenesis Assay. Human LECs were seeded on hydrogels with 7 mg mL^{-1} HA-Nor/BM polymer (2.63 mM BM) and cultured for 12 h in EGM MV2 media supplemented with 100 ng mL^{-1} VEGF-C, 50 ng mL^{-1} bFGF, and 1.5 μM S1P.[47] Images were acquired at 4× using an inverted light microscope (ECHO Revolve, San Diego, CA). Images were analyzed using kinetic analysis of vasculogenesis (KAV), a custom plug-in for FIJI.[57,58] To visualize lymphatic tube formation, human LECs cultured on hydrogels were fixed after 6 h, and samples were incubated with conjugated F-actin primary antibody and counterstained with DAPI. To visualize F-actin distribution and focal adhesion kinase (FAK), phalloidin and FAK antibodies were used.

4.15. LEC Gene Expression. To analyze the effect of hydrogel dynamics on lymphatic phenotypes, LECs were seeded on elastic and viscoelastic hydrogels and cultured for 12 h in EGM MV2 media, supplemented with 100 ng mL^{-1} VEGF-C, 50 ng mL^{-1} bFGF, and 1.5 μM S1P. The 12 h time point was selected to ensure that the signaling cascade in response to VEGF-C and mechanical stimulation was captured.[46,58] Each biological replicate was created by pooling RNA from three individual wells to collect a sufficient amount of RNA. At least three biological replicates (n = 3) were collected per condition and analyzed with real-time qRT-PCR with triplicate readings as previously described.[27] RNA was reverse transcribed using a high-capacity cDNA reverse transcription kit (Thermo Fisher) according to the manufacturer's protocol. cDNA was then used with the TaqMan Universal PCR Master Mix and Gene Expression Assays for *LYVE-1*, *PROX1*, *Podoplanin*, *VEGFR2*, *VEGFR3*, *NRP2*, *VE-CAD*, *MMP-1*, *MMP-2*, *MMP-14*, and *GAPDH*. Each sample was prepared in triplicate, and the relative expression was normalized to *GAPDH* and analyzed using the $^{\Delta\Delta}$Ct method.

4.16. Statistical Analysis. Statistical analysis was performed with GraphPad Prism 9.0 (GraphPad Software Inc., La Jolla, CA). All data were expressed as the mean ± standard deviation (SD). Statistical comparisons were performed using Student's t-test for paired data, analysis of variance (ANOVA) for multiple comparisons, and Tukey post hoc analysis for parametric data. Significance levels were set at the following: $^{**}p < 0.01$; $^{***}p < 0.001$; and $^{****}p < 0.0001$.

■ ASSOCIATED CONTENT

Supporting Information

The Supporting Information is available free of charge at https://pubs.acs.org/doi/10.1021/acsami.3c12514.

Synthesis route of BM-azide, HA-Nor, HA-BM, and HA-Nor/BM; NMR spectra; absorbance spectra; rheological data; photopatterning data; and cell viability data (PDF)

https://doi.org/10.1021/acsami.3c12514
ACS Appl. Mater. Interfaces 2023, 15, 58181−58195

AUTHOR INFORMATION

Corresponding Authors

Matthew J. Webber − *Chemical and Biomolecular Engineering, University of Notre Dame, Notre Dame, Indiana 46556, United States;* orcid.org/0000-0003-3111-6228; Email: mwebber@nd.edu

Donny Hanjaya-Putra − *Bioengineering Graduate Program, Aerospace and Mechanical Engineering, University of Notre Dame, Notre Dame, Indiana 46556, United States;* orcid.org/0000-0002-5403-544X; Email: dputra1@nd.edu

Authors

Fei Fan − *Bioengineering Graduate Program, Aerospace and Mechanical Engineering, University of Notre Dame, Notre Dame, Indiana 46556, United States*

Bo Su − *Chemical and Biomolecular Engineering, University of Notre Dame, Notre Dame, Indiana 46556, United States*

Alexander Kolodychak − *Chemical and Biomolecular Engineering, University of Notre Dame, Notre Dame, Indiana 46556, United States*

Ephraim Ekwueme − *Bioengineering Graduate Program, Aerospace and Mechanical Engineering, University of Notre Dame, Notre Dame, Indiana 46556, United States*

Laura Alderfer − *Bioengineering Graduate Program, Aerospace and Mechanical Engineering, University of Notre Dame, Notre Dame, Indiana 46556, United States*

Sanjoy Saha − *Bioengineering Graduate Program, Aerospace and Mechanical Engineering, University of Notre Dame, Notre Dame, Indiana 46556, United States*

Complete contact information is available at: https://pubs.acs.org/10.1021/acsami.3c12514

Author Contributions

F.F., M.J.W., and D.H.-P. conceived the ideas, designed the experiments, interpreted the data, and wrote the manuscript. F.F., B.S., A.K., E.E., L.A., and S.S. conducted the experiments and analyzed the data. All authors have approved the manuscript.

Notes

The authors declare no competing financial interest.

ACKNOWLEDGMENTS

The authors acknowledge support from the University of Notre Dame through the "Advancing Our Vision" Initiative in stem cell research, the American Heart Association through Career Development Award (19-CDA-34630012 to D.H.-P.), the National Institute of Health (R35GM143055 to D.H.-P. and R35GM137987 to M.J.W.), and the National Science Foundation (CBET, 2047903 to D.H.-P. and BMAT, 1944875 to M.J.W). The authors would like to thank the Center for Environmental Science and Technology and the ND Energy Materials Characterization Core for help with material characterization.

REFERENCES

(1) Rosales, A. M.; Anseth, K. S. The Design of Reversible Hydrogels to Capture Extracellular Matrix Dynamics. *Nat. Rev. Mater.* **2016**, *1* (2), 15012.

(2) Lewis, G. Viscoelastic Properties of Injectable Bone Cements for Orthopaedic Applications: State-of-the-Art Review. *J. Biomed. Mater. Res., Part B* **2011**, *98* (1), 171−191.

(3) Rassoli, A.; Fatouraee, N.; Guidoin, R. Structural Model for Viscoelastic Properties of Pericardial Bioprosthetic Valves. *Artif. Organs* **2018**, *42* (6), 630−639.

(4) Demirci, N.; Jafarabadi, F.; Wang, X.; Wang, S.; Holland, M. A. Consistency and Variation in the Placement of Cortical Folds: A Perspective. *Brain Multiphys.* **2023**, *5*, No. 100080.

(5) Juliar, B. A.; Strieder-Barboza, C.; Karmakar, M.; Flesher, C. G.; Baker, N. A.; Varban, O. A.; Lumeng, C. N.; Putnam, A. J.; O'Rourke, R. W. Viscoelastic Characterization of Diabetic and Non-Diabetic Human Adipose Tissue. *Biorheology* **2020**, *57* (1), 15−26.

(6) Streitberger, K.-J.; Reiss-Zimmermann, M.; Freimann, F. B.; Bayerl, S.; Guo, J.; Arlt, F.; Wuerfel, J.; Braun, J.; Hoffmann, K.-T.; Sack, I. High-Resolution Mechanical Imaging of Glioblastoma by Multifrequency Magnetic Resonance Elastography. *PLoS One* **2014**, *9* (10), No. e110588.

(7) Nabavizadeh, A.; Bayat, M.; Kumar, V.; Gregory, A.; Webb, J.; Alizad, A.; Fatemi, M. Viscoelastic Biomarker for Differentiation of Benign and Malignant Breast Lesion in Ultra- Low Frequency Range. *Sci. Rep* **2019**, *9* (1), No. 5737.

(8) Ma, Y.; Han, T.; Yang, Q.; Wang, J.; Feng, B.; Jia, Y.; Wei, Z.; Xu, F. Viscoelastic Cell Microenvironment: Hydrogel-Based Strategy for Recapitulating Dynamic ECM Mechanics. *Adv. Funct. Mater.* **2021**, *31* (24), No. 2100848.

(9) Webber, M. J.; Tibbitt, M. W. Dynamic and Reconfigurable Materials from Reversible Network Interactions. *Nat. Rev. Mater.* **2022**, *7* (7), 541−556.

(10) Mantooth, S. M.; Munoz-Robles, B. G.; Webber, M. J. Dynamic Hydrogels from Host−Guest Supramolecular Interactions. *Macromol. Biosci.* **2019**, *19* (1), No. 1800281.

(11) Zou, L.; Braegelman, A. S.; Webber, M. J. Dynamic Supramolecular Hydrogels Spanning an Unprecedented Range of Host−Guest Affinity. *ACS Appl. Mater. Interfaces* **2019**, *11* (6), 5695−5700.

(12) Rodell, C. B.; Kaminski, A. L.; Burdick, J. A. Rational Design of Network Properties in Guest−Host Assembled and Shear-Thinning Hyaluronic Acid Hydrogels. *Biomacromolecules* **2013**, *14* (11), 4125−4134.

(13) Widener, A. E.; Bhatta, M.; Angelini, T. E.; Phelps, E. A. Guest−Host Interlinked PEG-MAL Granular Hydrogels as an Engineered Cellular Microenvironment. *Biomater. Sci.* **2021**, *9* (7), 2480−2493.

(14) Rodell, C. B.; MacArthur, J. W.; Dorsey, S. M.; Wade, R. J.; Wang, L. L.; Woo, Y. J.; Burdick, J. A. Shear-Thinning Supramolecular Hydrogels with Secondary Autonomous Covalent Crosslinking to Modulate Viscoelastic Properties In Vivo. *Adv. Funct. Mater.* **2015**, *25* (4), 636−644.

(15) Nam, S.; Stowers, R.; Lou, J.; Xia, Y.; Chaudhuri, O. Varying PEG Density to Control Stress Relaxation in Alginate-PEG Hydrogels for 3D Cell Culture Studies. *Biomaterials* **2019**, *200*, 15−24.

(16) Marozas, I. A.; Anseth, K. S.; Cooper-White, J. J. Adaptable Boronate Ester Hydrogels with Tunable Viscoelastic Spectra to Probe Timescale Dependent Mechanotransduction. *Biomaterials* **2019**, *223*, No. 119430.

(17) Tang, S.; Ma, H.; Tu, H.-C.; Wang, H.-R.; Lin, P.-C.; Anseth, K. S. Adaptable Fast Relaxing Boronate-Based Hydrogels for Probing Cell−Matrix Interactions. *Adv. Sci.* **2018**, *5* (9), No. 1800638.

(18) Figueiredo, T.; Jing, J.; Jeacomine, I.; Olsson, J.; Gerfaud, T.; Boiteau, J.-G.; Rome, C.; Harris, C.; Auzély-Velty, R. Injectable Self-Healing Hydrogels Based on Boronate Ester Formation between Hyaluronic Acid Partners Modified with Benzoxaborin Derivatives and Saccharides. *Biomacromolecules* **2020**, *21* (1), 230−239.

(19) Yesilyurt, V.; Ayoob, A. M.; Appel, E. A.; Borenstein, J. T.; Langer, R.; Anderson, D. G. Mixed Reversible Covalent Crosslink Kinetics Enable Precise, Hierarchical Mechanical Tuning of Hydrogel Networks. *Adv. Mater.* **2017**, *29* (19), No. 1605947.

(20) Chaudhuri, O.; Gu, L.; Darnell, M.; Klumpers, D.; Bencherif, S. A.; Weaver, J. C.; Huebsch, N.; Mooney, D. J. Substrate Stress Relaxation Regulates Cell Spreading. *Nat. Commun.* **2015**, *6* (1), No. 6365.

(21) Bauer, A.; Gu, L.; Kwee, B.; Li, W. A.; Dellacherie, M.; Celiz, A. D.; Mooney, D. J. Hydrogel Substrate Stress-Relaxation Regulates the Spreading and Proliferation of Mouse Myoblasts. *Acta Biomater.* **2017**, *62*, 82−90.
(22) Cameron, A. R.; Frith, J. E.; Gomez, G. A.; Yap, A. S.; Cooper-White, J. J. The Effect of Time-Dependent Deformation of Viscoelastic Hydrogels on Myogenic Induction and Rac1 Activity in Mesenchymal Stem Cells. *Biomaterials* **2014**, *35* (6), 1857−1868.
(23) Lee, H.-p.; Stowers, R.; Chaudhuri, O. Volume Expansion and TRPV4 Activation Regulate Stem Cell Fate in Three-Dimensional Microenvironments. *Nat. Commun.* **2019**, *10* (1), No. 529.
(24) Chaudhuri, O.; Gu, L.; Klumpers, D.; Darnell, M.; Bencherif, S. A.; Weaver, J. C.; Huebsch, N.; Lee, H.; Lippens, E.; Duda, G. N.; Mooney, D. J. Hydrogels with Tunable Stress Relaxation Regulate Stem Cell Fate and Activity. *Nat. Mater.* **2016**, *15* (3), 326−334.
(25) Indana, D.; Agarwal, P.; Bhutani, N.; Chaudhuri, O. Viscoelasticity and Adhesion Signaling in Biomaterials Control Human Pluripotent Stem Cell Morphogenesis in 3D Culture. *Adv. Mater.* **2021**, *33* (43), No. 2101966.
(26) Wei, Z.; Schnellmann, R.; Pruitt, H. C.; Gerecht, S. Hydrogel Network Dynamics Regulate Vascular Morphogenesis. *Cell Stem Cell* **2020**, *27* (5), 798−812.e6.
(27) Zou, L.; Webber, M. J. Reversible Hydrogel Dynamics by Physical−Chemical Crosslink Photoswitching Using a Supramolecular Macrocycle Template. *Chem. Commun.* **2019**, *55* (67), 9931−9934.
(28) Zou, L.; Su, B.; Addonizio, C. J.; Pramudya, I.; Webber, M. J. Temperature-Responsive Supramolecular Hydrogels by Ternary Complex Formation with Subsequent Photo-Cross-Linking to Alter Network Dynamics. *Biomacromolecules* **2019**, *20* (12), 4512−4521.
(29) Gramlich, W. M.; Kim, I. L.; Burdick, J. A. Synthesis and Orthogonal Photopatterning of Hyaluronic Acid Hydrogels with Thiol-Norbornene Chemistry. *Biomaterials* **2013**, *34* (38), 9803−9811.
(30) Vega, S. L.; Kwon, M. Y.; Song, K. H.; Wang, C.; Mauck, R. L.; Han, L.; Burdick, J. A. Combinatorial Hydrogels with Biochemical Gradients for Screening 3D Cellular Microenvironments. *Nat. Commun.* **2018**, *9* (1), No. 614.
(31) Highley, C. B.; Prestwich, G. D.; Burdick, J. A. Recent Advances in Hyaluronic Acid Hydrogels for Biomedical Applications. *Curr. Opin. Biotechnol.* **2016**, *40*, 35−40.
(32) Burdick, J. A.; Prestwich, G. D. Hyaluronic Acid Hydrogels for Biomedical Applications. *Adv. Mater.* **2011**, *23* (12), H41−H56.
(33) Fan, F.; Zhang, P.; Wang, L.; Sun, T.; Cai, C.; Yu, G. Synthesis and Properties of Functional Glycomimetics through Click Grafting of Fucose onto Chondroitin Sulfates. *Biomacromolecules* **2019**, *20* (10), 3798−3808.
(34) Kunishima, M.; Kawachi, C.; Monta, J.; Terao, K.; Iwasaki, F.; Tani, S. 4-(4,6-Dimethoxy-1,3,5-Triazin-2-Yl)-4-Methyl-Morpholinium Chloride: An Efficient Condensing Agent Leading to the Formation of Amides and Esters. *Tetrahedron* **1999**, *55* (46), 13159−13170.
(35) Kang, Y.; Tang, X.; Yu, H.; Cai, Z.; Huang, Z.; Wang, D.; Xu, J.-F.; Zhang, X. Supramolecular Catalyst Functions in Catalytic Amount: Cucurbit[8]Uril Accelerates the Photodimerization of Brooker's Merocyanine. *Chem. Sci.* **2017**, *8* (12), 8357−8361.
(36) Tabet, A.; Forster, R. A.; Parkins, C. C.; Wu, G.; Scherman, O. A. Modulating Stiffness with Photo-Switchable Supramolecular Hydrogels. *Polym. Chem.* **2019**, *10* (4), 467−472.
(37) Niu, W.; Guo, L.; Li, Y.; Shuang, S.; Dong, C.; Wong, M. S. Highly Selective Two-Photon Fluorescent Probe for Ratiometric Sensing and Imaging Cysteine in Mitochondria. *Anal. Chem.* **2016**, *88* (3), 1908−1914.
(38) Zhang, H.; Li, M.; Zhang, C.; Zhang, G.; Chao, J.; Shi, L.; Yao, Q.; Shuang, S.; Dong, C. The Design of Hydrogen Sulfide Fluorescence Probe Based on Dual Nucleophilic Reaction and Its Application for Bioimaging. *Spectrochim. Acta, Part A* **2019**, *207*, 150−155.
(39) Heilemann, M.; Dedecker, P.; Hofkens, J.; Sauer, M. Photoswitches: Key Molecules for Subdiffraction-Resolution Fluorescence Imaging and Molecular Quantification. *Laser Photonics Rev.* **2009**, *3* (1−2), 180−202.
(40) Dempsey, G. T.; Bates, M.; Kowtoniuk, W. E.; Liu, D. R.; Tsien, R. Y.; Zhuang, X. Photoswitching Mechanism of Cyanine Dyes. *J. Am. Chem. Soc.* **2009**, *131* (51), 18192−18193.
(41) Gidi, Y.; Payne, L.; Glembockyte, V.; Michie, M. S.; Schnermann, M. J.; Cosa, G. Unifying Mechanism for Thiol-Induced Photoswitching and Photostability of Cyanine Dyes. *J. Am. Chem. Soc.* **2020**, *142* (29), 12681−12689.
(42) Chen, H.; Zhang, J.; Yu, W.; Cao, Y.; Cao, Z.; Tan, Y. Control Viscoelasticity of Polymer Networks with Crosslinks of Superposed Fast and Slow Dynamics. *Angew. Chem., Int. Ed.* **2021**, *60* (41), 22332−22338.
(43) Lou, J.; Friedowitz, S.; Will, K.; Qin, J.; Xia, Y. Predictably Engineering the Viscoelastic Behavior of Dynamic Hydrogels via Correlation with Molecular Parameters. *Adv. Mater.* **2021**, *33* (51), No. 2104460.
(44) DiMaio, J. T. M.; Doran, T. M.; Ryan, D. M.; Raymond, D. M.; Nilsson, B. L. Modulating Supramolecular Peptide Hydrogel Viscoelasticity Using Biomolecular Recognition. *Biomacromolecules* **2017**, *18* (11), 3591−3599.
(45) Hui, E.; Gimeno, K. I.; Guan, G.; Caliari, S. R. Spatiotemporal Control of Viscoelasticity in Phototunable Hyaluronic Acid Hydrogels. *Biomacromolecules* **2019**, *20* (11), 4126−4134.
(46) Alderfer, L.; Russo, E.; Archilla, A.; Coe, B.; Hanjaya-Putra, D. Matrix Stiffness Primes Lymphatic Tube Formation Directed by Vascular Endothelial Growth Factor-C. *FASEB J.* **2021**, *35*, No. e57044, DOI: 10.1096/fj.202002426RR.
(47) Hanjaya-Putra, D.; Bose, V.; Shen, Y.-I.; Yee, J.; Khetan, S.; Fox-Talbot, K.; Steenbergen, C.; Burdick, J. A.; Gerecht, S. Controlled Activation of Morphogenesis to Generate a Functional Human Microvasculature in a Synthetic Matrix. *Blood* **2011**, *118* (3), 804−815.
(48) Alderfer, L.; Wei, A.; Hanjaya-Putra, D. Lymphatic Tissue Engineering and Regeneration. *J. Biol. Eng.* **2018**, *12* (1), 32.
(49) Hanjaya-Putra, D.; Yee, J.; Ceci, D.; Truitt, R.; Yee, D.; Gerecht, S. Vascular Endothelial Growth Factor and Substrate Mechanics Regulate in Vitro Tubulogenesis of Endothelial Progenitor Cells. *J. Cell. Mol. Med.* **2010**, *14* (10), 2436−2447.
(50) Hooks, J. S. T.; Bernard, F. C.; Cruz-Acuña, R.; Nepiyushchikh, Z.; Gonzalez-Vargas, Y.; García, A. J.; Dixon, J. B. Synthetic Hydrogels Engineered to Promote Collecting Lymphatic Vessel Sprouting. *Biomaterials* **2022**, *284*, No. 121483.
(51) Mukherjee, A.; Hooks, J.; Nepiyushchikh, Z.; Dixon, J. B. Entrainment of Lymphatic Contraction to Oscillatory Flow. *Sci. Rep.* **2019**, *9* (1), 5840.
(52) Ruliffson, B. N. K.; Whittington, C. F. Regulating Lymphatic Vasculature in Fibrosis: Understanding the Biology to Improve the Modeling. *Adv. Biol.* **2023**, *7* (5), No. 2200158.
(53) Alderfer, L.; Hall, E.; Hanjaya-Putra, D. Harnessing Biomaterials for Lymphatic System Modulation. *Acta Biomater.* **2021**, *133*, 34−45.
(54) Frye, M.; Taddei, A.; Dierkes, C.; Martinez-Corral, I.; Fielden, M.; Ortsäter, H.; Kazenwadel, J.; Calado, D. P.; Ostergaard, P.; Salminen, M.; He, L.; Harvey, N. L.; Kiefer, F.; Mäkinen, T. Matrix Stiffness Controls Lymphatic Vessel Formation through Regulation of a GATA2-Dependent Transcriptional Program. *Nat. Commun.* **2018**, *9* (1), No. 1511.
(55) Bayless, K. J.; Kwak, H.-I.; Su, S.-C. Investigating Endothelial Invasion and Sprouting Behavior in Three-Dimensional Collagen Matrices. *Nat. Protoc.* **2009**, *4* (12), 1888−1898.
(56) Hanjaya-Putra, D.; Wong, K. T.; Hirotsu, K.; Khetan, S.; Burdick, J. A.; Gerecht, S. Spatial Control of Cell-Mediated Degradation to Regulate Vasculogenesis and Angiogenesis in Hyaluronan Hydrogels. *Biomaterials* **2012**, *33* (26), 6123−6131.
(57) Varberg, K. M.; Winfree, S.; Chu, C.; Tu, W.; Blue, E. K.; Gohn, C. R.; Dunn, K. W.; Haneline, L. S. Kinetic Analyses of Vasculogenesis Inform Mechanistic Studies. *Am. J. Physiol.: Cell Physiol.* **2017**, *312* (4), C446−C458.

(58) Bui, L.; Edwards, S.; Hall, E.; Alderfer, L.; Round, K.; Owen, M.; Sainaghi, P.; Zhang, S.; Nallathamby, P. D.; Haneline, L. S.; Hanjaya-Putra, D. Engineering Bioactive Nanoparticles to Rejuvenate Vascular Progenitor Cells. *Commun. Biol.* **2022**, *5* (1), 635.
(59) Banerji, S.; Ni, J.; Wang, S.-X.; Clasper, S.; Su, J.; Tammi, R.; Jones, M.; Jackson, D. G. LYVE-1, a New Homologue of the CD44 Glycoprotein, Is a Lymph-Specific Receptor for Hyaluronan. *J. Cell Biol.* **1999**, *144* (4), 789 LP−801.
(60) Jeong, D. P.; Hall, E.; Neu, E.; Hanjaya-Putra, D. Podoplanin Is Responsible for the Distinct Blood and Lymphatic Capillaries. *Cell. Mol. Bioeng.* **2022**, *15*, No. 467.
(61) Schacht, V.; Ramirez, M. I.; Hong, Y.-K.; Hirakawa, S.; Feng, D.; Harvey, N.; Williams, M.; Dvorak, A. M.; Dvorak, H. F.; Oliver, G.; Detmar, M. T1α/Podoplanin Deficiency Disrupts Normal Lymphatic Vasculature Formation and Causes Lymphedema. *EMBO J.* **2003**, *22* (14), 3546−3556.
(62) Osada, M.; Inoue, O.; Ding, G.; Shirai, T.; Ichise, H.; Hirayama, K.; Takano, K.; Yatomi, Y.; Hirashima, M.; Fujii, H.; Suzuki-Inoue, K.; Ozaki, Y. Platelet Activation Receptor CLEC-2 Regulates Blood/Lymphatic Vessel Separation by Inhibiting Proliferation, Migration, and Tube Formation of Lymphatic Endothelial Cells. *J. Biol. Chem.* **2012**, *287*, No. 22241.
(63) Jeong, D. P.; Daniel Montes, P.; Chang, H.-C.; Hanjaya-Putra, D. Fractal Dimension to Characterize Interactions between Blood and Lymphatic Endothelial Cells. *Phys. Biol.* **2023**, *20*, No. 045004, DOI: 10.1088/1478-3975/acd898.
(64) Wigle, J. T.; Oliver, G. Prox1 Function Is Required for the Development of the Murine Lymphatic System. *Cell* **1999**, *98* (6), 769−778.
(65) Oliver, G.; Srinivasan, R. S. Endothelial Cell Plasticity: How to Become and Remain a Lymphatic Endothelial Cell. *Development* **2010**, *137* (3), 363−372.
(66) Xu, Y.; Yuan, L.; Mak, J.; Pardanaud, L.; Caunt, M.; Kasman, I.; Larrivée, B.; del Toro, R.; Suchting, S.; Medvinsky, A.; Silva, J.; Yang, J.; Thomas, J.-L.; Koch, A. W.; Alitalo, K.; Eichmann, A.; Bagri, A. Neuropilin-2 Mediates VEGF-C−Induced Lymphatic Sprouting Together with VEGFR3. *J. Cell Biol.* **2010**, *188* (1), 115−130.
(67) Favier, B.; Alam, A.; Barron, P.; Bonnin, J.; Laboudie, P.; Fons, P.; Mandron, M.; Herault, J.-P.; Neufeld, G.; Savi, P.; Herbert, J.-M.; Bono, F. Neuropilin-2 Interacts with VEGFR-2 and VEGFR-3 and Promotes Human Endothelial Cell Survival and Migration. *Blood* **2006**, *108* (4), 1243−1250.
(68) Hägerling, R.; Hoppe, E.; Dierkes, C.; Stehling, M.; Makinen, T.; Butz, S.; Vestweber, D.; Kiefer, F. Distinct Roles of VE-Cadherin for Development and Maintenance of Specific Lymph Vessel Beds. *EMBO J.* **2018**, *37* (22), No. e98271.
(69) Harris, N. R.; Nielsen, N. R.; Pawlak, J. B.; Aghajanian, A.; Rangarajan, K.; Serafin, D. S.; Farber, G.; Dy, D. M.; Nelson-Maney, N. P.; Xu, W.; Ratra, D.; Hurr, S. H.; Qian, L.; Scallan, J. P.; Caron, K. M. VE-Cadherin Is Required for Cardiac Lymphatic Maintenance and Signaling. *Circ. Res.* **2022**, *130* (1), 5−23.
(70) Nakashima, B. J.; Hong, Y.-K. VE-Cadherin: A Critical Sticking Point for Lymphatic System Maintenance: Role of VE-Cadherin in Lymphatic Maintenance. *Circ. Res.* **2022**, *130* (1), 24−26.
(71) Saha, S.; Fan, F.; Alderfer, L.; Graham, F.; Hall, E.; Hanjaya-Putra, D. Synthetic Hyaluronic Acid Coating Preserves the Phenotypes of Lymphatic Endothelial Cells. *Biomater. Sci.* **2023**, *11* (22), 7346−7357.

https://doi.org/10.1021/acsami.3c12514
ACS Appl. Mater. Interfaces 2023, 15, 58181−58195